Available online at www.sciencedirect.com
SCIENCE DIRECT®
PERGAMON
International Journal of Heat and Mass Transfer 46 (2003) 3365–3387
International Journal of HEAT and MASS TRANSFER
www.elsevier.com/locate/ijhmt

# Condensation in horizontal tubes, part 2: new heat transfer model based on flow regimes

J.R. Thome [a,*], J. El Hajal [a], A. Cavallini [b]

[a] *Laboratory of Heat and Mass Transfer, Faculty of Engineering Science, Swiss Federal Institute of Technology, Lausanne, CH-1015 Lausanne, Switzerland*

[b] *Dipartimento di Fisca Tecnica, University of Padova, Padova, I-35131, Italy*

Received 24 June 2002; received in revised form 4 March 2003

**Abstract**

A new general flow pattern/flow structure based heat transfer model for condensation inside horizontal, plain tubes is proposed based on simplified flow structures of the flow regimes, and also includes the effect of liquid–vapor interfacial roughness on heat transfer. The model predicts local condensation heat transfer coefficients for the following flow regimes: annular, intermittent, stratified-wavy, fully stratified and mist flow. The new model has been compared to test data for 15 fluids (R-11, R-12, R-22, R-32, R-113, R-125, R-134a, R-236ea, a R-32/R-125 near-azeotrope, R-404A, R-410A, propane, *n*-butane, iso-butane and propylene) obtained in nine independent research laboratories. The new model has been tested over the following range of conditions: mass velocities from 24 to 1022 kg/(m$^2$ s), vapor qualities from 0.03 to 0.97, reduced pressures from 0.02 to 0.80 and tube internal diameters from 3.1 to 21.4 mm. Overall, the model predicts 85% of the heat transfer coefficients in the non-hydrocarbon database (1850 points) to within ±20% with nearly uniform accuracy for each flow regime and predicts 75% of the entire database to within ±20% when including the hydrocarbons (2771 points), the latter all from a single laboratory whose data had some unusual experimental trends over part of their test range.


*Keywords:* Intube condensation; Heat transfer model; Refrigerants; Hydrocarbons

## 1. Introduction

In the second half of the past century, numerous models have been proposed in the literature to predict local heat transfer coefficients for condensation of pure saturated vapors under forced convection conditions inside plain horizontal tubes. These methods have only been partially successful because of the limited databases used, use of poor or overly simplistic transition criteria between the stratified flows and non-stratified flows, and so forth. In Part I of this two-part paper, a new flow pattern map and void fraction equation were proposed for condensation. In this part, that map and void fraction equation are used to proposed a new flow patterned based condensation heat transfer model for condensation inside horizontal, plain tubes. The objective is to obtain a method with a minimum of empirical constants and exponents that not only gives a good statistical representation of the data, but also correctly captures the trends in the data. This latter point is particularly important when such a method is used in an optimization program for the design of air-cooled condensers. The basic idea here is to adapt the principles used in the flow pattern-based intube flow *boiling* heat transfer model of Kattan et al. [1–3] for predicting intube *condensation* heat transfer.

* Corresponding author. Tel.: +41-21-693-5981; fax: +41-21-693-5960.

*E-mail addresses:* john.thome@epfl.ch (J.R. Thome), jean.elhajal@epfl.ch (J. El Hajal), alcav@unipd.it (A. Cavallini).

0017-9310/03/$ - see front matter 
doi:10.1016/S0017-9310(03)00140-6

**Nomenclature**

| | |
|---|---|
| $A$ | total cross-sectional area of tube ($m^2$) |
| $A_L$ | cross-sectional area of tube occupied by liquid ($m^2$) |
| $A_V$ | cross-sectional area of tube occupied by vapor ($m^2$) |
| $c$ | convective film constant (–) |
| $c_{pL}$ | liquid specific heat (J/(kg K)) |
| $d$ | internal tube diameter (m) |
| $f_i$ | interfacial roughness factor (–) |
| $g$ | acceleration of gravity ($m/s^2$) |
| $G$ | total mass velocity of liquid and vapor (kg/($m^2$ s)) |
| $G_{bubbly}$ | bubbly flow transition mass velocity (kg/($m^2$ s)) |
| $G_{mist}$ | mist flow transition mass velocity (kg/($m^2$ s)) |
| $G_{strat}$ | stratified flow transition mass velocity (kg/($m^2$ s)) |
| $G_{wavy}$ | wavy flow transition mass velocity (kg/($m^2$ s)) |
| $h_{LG}$ | latent heat of vaporization (J/kg) |
| $j$ | exponent ($j = 1/2$) (–) |
| $k$ | exponent ($k = 1/4$) (–) |
| $m$ | exponent on $Pr_L$ (–) |
| $n$ | exponent on $Re_L$ (–) |
| $p_{crit}$ | critical pressure ($N/m^2$) |
| $p_r$ | reduced pressure ($p_r = p_{sat}/p_{crit}$) (–) |
| $p_{sat}$ | saturation pressure ($N/m^2$) |
| $Pr_L$ | liquid Prandtl number (–) |
| $q$ | heat flux from fluid to tube ($W/m^2$) |
| $r$ | internal radius of tube (m) |
| $Re_L$ | Reynolds number of liquid film (–) |
| $T_{sat}$ | saturation temperature (K) |
| $T_w$ | wall temperature (K) |
| $\Delta T_{water}$ | fall in water temperature from inlet to outlet (K) |
| $u_L$ | mean liquid velocity in film (m/s) |
| $u_V$ | mean vapor velocity (m/s) |
| $x$ | vapor quality (–) |
| $x_{IA}$ | vapor quality at transition from intermittent to annular flow (–) |
| $\Delta x$ | change in vapor quality from inlet to outlet (–) |
| $X_{tt}$ | Martinelli parameter with both phases turbulent [–] |

*Greek symbols*

| | |
|---|---|
| $\alpha_c$ | convective condensation heat transfer coefficient ($W/(m^2 K)$) |
| $\alpha_{cb}$ | convective boiling heat transfer coefficient ($W/(m^2 K)$) |
| $\alpha_f$ | Nusselt film condensing coefficient on top perimeter of tube ($W/(m^2 K)$) |
| $\alpha_{tp}$ | local perimeter averaged condensing heat transfer coefficient ($W/(m^2 K)$) |
| $\delta$ | liquid film thickness of annular ring (m) |
| $\delta_{in}$ | initial liquid film thickness after desuperheating zone (m) |
| $\Delta\delta_i$ | interfacial roughness (m) |
| $\varepsilon$ | void fraction of vapor (–) |
| $\lambda_L$ | liquid thermal conductivity (W/(m K)) |
| $\lambda_T$ | Taylor instability wavelength (m) |
| $\mu_L$ | liquid dynamic viscosity ($N s/m^2$) |
| $\theta$ | upper angle of the tube not wetted by stratified liquid (rad) |
| $\theta_{strat}$ | stratified angle around upper perimeter of the tube (rad) |
| $\rho_G$ | vapor density ($kg/m^3$) |
| $\rho_L$ | liquid density ($kg/m^3$) |
| $\sigma$ | surface tension (N/m) |
| $\tau_i$ | interfacial shear of vapor on liquid film ($J/m^3$) |

## 2. Literature review of condensation models

In the early models, the flow patterns were classified under only two categories, as either *stratified* (or *stratifying*, or *wavy*) flow or as *annular* flow. In the first case, the gravity dominated flow has been modelled considering a thick condensate layer flowing along the bottom of the tube, while a thin liquid film forms on the wall in the upper portion of the tube. Heat transfer through the thin film is treated by a classical Nusselt type analysis, while heat transfer through the thick condensate layer can either be neglected as in Jaster and Kosky [4], or treated as a convective process. In the shear dominated *annular* flow, two different approaches were used for the calculation of heat transfer coefficients: an interfacial shear model or a two-phase multiplier correlation. The latter is the most common approach consisting in calculating the Nusselt number during condensation by multiplying the Nusselt number for turbulent single-phase flow by a suitable two-phase multiplier. The two-phase multiplier is usually given as a function of some of the following parameters: vapor quality, viscosity and density ratios between the liquid and vapor phases, reduced pressure, liquid Froude number, Martinelli $X_{tt}$ parameter, etc. For the single-phase Nusselt number upon which these multipliers act, the equation by Dittus and Boelter [5] is often the basis.

Worth mentioning, although very old, are the equations by Akers et al. [6] and Akers and Rosson [7], still recommended as a design tool in the ASHRAE Handbook [8]. Three straightforward equations are given, each of them applicable within definite ranges of suitable dimensionless parameters; they cover both annular and stratified flow conditions. The one for annular flow is of the two-phase multiplier type. Cavallini and Zecchin [9] proposed a simple dimensionless semi-empirical equation to be applied when annular flow is present during condensation. The same authors showed later [10] that their equation represented, within narrow limits, the results of a flow-dynamic analysis of the condensation phenomenon. Similar analyses, based on the assumption that the Von Karman velocity profile for pipe flow holds true in the condensate annulus, had previously been used by Kosky and Staub [11] and Traviss et al. [12], to develop their own calculation procedures, valid of course only with an annular flow pattern. The method by Kosky and Staub is for instance recommended by Butterworth [13] in the *Heat Transfer Design Handbook*. Analyses based on a similar type of approach are also suggested for design purposes in Germany in their VDI Wärmeatlas, i.e. *VDI Heat Atlas* [14] translated in English, and still in the most recent version in German, *VDI Wärmeatlas* [15]. A two-phase multiplier correlation extensively used in North America is the one by Shah [16], which should coherently be applied only in the presence of an annular flow pattern, even if the author did not establish this limitation, presenting his expression as a ''generalised'' one.

Tang [17], based on his condensation measurements, also developed a new heat transfer two-phase multiplier correlation valid in the annular flow regime, when mass velocities are larger than 300 kg/(m$^2$ s) and the reduced pressure is between 0.2 and 0.53. The computational method suggested by Haraguchi et al. [18] is extensively used in Japan. It consists of two dimensionless equations, one each for both annular and stratified flow conditions, combined together in an asymptotic way. Appropriate applicability ranges are specified. Dobson and Chato [19] presented a set of equations able to predict the heat transfer coefficient both in the stratified flow regime and in the annular one; the annular flow correlation was derived using the two-phase multiplier approach. In some circumstances quite discontinuous results are calculated when passing from one flow regime to the other, contrary to experimental evidence.

Recently, Cavallini et al. [20] compared most of the above prediction methods to heat transfer coefficients of halogenated refrigerants condensing inside horizontal plain tubes, for experimental data obtained by independent research workers. The outcome of this comparison showed that a few of the above methods, when employed with condensation of the old generation refrigerants, were able to predict satisfactorily the experimental data, that is generally within ±20%. This applies in particular, with somewhat different approximations, to the methods by Shah, Cavallini-Zecchin, Dobson-Chato, Tang, Traviss et al. and Haraguchi et al. Nevertheless, this did not hold true when the same methods were applied to condensation of some of the new generation HFC refrigerants, those that are commonly used at higher pressure (also higher reduced pressure) than the traditional refrigerants. In this case the available predicting methods, developed in the past in connection with availability of experimental data only concerning traditional refrigerants, either cannot be applied because of the cited limits in their application ranges, or unacceptably overpredict the experimental data, typically by 20–40%. To overcome this situation, Cavallini et al. [20] presented a new heat transfer flow pattern-based method, that was able to give satisfactory predictions also with the new generation high-pressure refrigerants while their flow pattern map was discussed in Part I of this two-part paper. In the annular flow regime, the method employs an interfacial shear model similar to that developed by Kosky and Staub [11], with a modified Friedel [21] correlation for the calculation of the frictional pressure drop and related wall shear stress. For their comparison, Cavallini et al. [20] used an extensive experimental data bank formed from quite a few data sets taken in independent research laboratories. Details of this data bank are reported in Table 1, where they represent the first nine listings. While their new model was an improvement upon past methods, it also included a large number of empirical constants and also predicts an unlikely jump in the heat transfer coefficient across one flow transition boundary. Hence, the objective here is to present a new condensation heat transfer model that avoids these pitfalls and also will predict hydrocarbon data.

## 3. Heat transfer database

The database of condensation heat transfer coefficients available for the current study is described in Table 1. These studies are contributions from nine independent research laboratories and cover 15 fluids and a wide range of test conditions. Only studies from the 1990s to the present have been considered as they are more accurate than the older databases, i.e. newer studies use Coriolis mass flow meters for both the coolant and the refrigerant, more accurate data acquisition systems and so on. The newest study, that of Liebenberg [29], only includes his R-22 data available at this time.

This list of test fluids includes single component refrigerants (R-11, R-12, R-22, R-32, R-113, R-125, R-134a, R-236ea), binary azeotropic or very near azeotropic refrigerant mixtures (60% R-32/40% R-125,

Table 1
Condensation heat transfer data bank (pure fluids and quasi-azeotropic mixtures)

| Author(s) | Data points | Refrigerants | $d$ (mm) | $T_{sat}$ (°C) | $T_{sat} - T_w$ (°C) | $G$ (kg/(m$^2$ s)) |
|---|---|---|---|---|---|---|
| Cavallini et al. [22,23] | 425 | R-22, R-134a, R-410A, R-125, R-32, R-236ea | 8.0 | 27–60 | 2.4–15.4 | 63–773 |
| Dobson–Chato [19] | 644 | R-22, R-134a, R-410A, R-32/R-125 (60/40% by mass) | 3.1–7.0 | 33.5–46.4 | 1.1–8.8 | 24–812 |
| Zhang [24] | 77 | R-22, R-134a, R-404A | 3.3–6.2 | 23.1–65.2 | 1.0–5.6 | 245–1022 |
| Tang [17] | 218 of 231* | R-22, R-134a, R-410A | 8.8 | 35.2–40.8 | – | 258–817 |
| Chitti–Anand [25] | 41 of 48* | R-410A | 8.0 | 24–36 | – | 161–491 |
| Kim et al. [26] | 225 | R-22 | 8.0 | 48–49 | 2.7–9.6 | 229–343 |
| Kim et al. [26] | 921 | Propane, *n*-Butane, iso-Butane, Propylene | 8.0 | 46.6–50.2 | 1.2–9.8 | 44–204 |
| Wijaya–Spatz [27] | 14 | R-410A | 7.8 | 46–52 | – | 481 |
| Fujii [28] | 158 | R-11, R-12, R-113 | 16.0–21.4 | 28.4–50.1 | 2.2–32.7 | 33–577 |
| Liebenberg [29] | 48 of 50* | R-22 | 8.11 | 38.4–43.2 | – | 304–832 |

Data marked with * refers to data which could not be used because they fell in a flow regime requiring experimental measurement of $(T_{sat} - T_w)$ which were not reported.

R-404A, R-410A) and pure hydrocarbons (propane, *n*-butane, iso-butane and propylene). The database covers a very broad range of conditions: mass velocities from 24 to 1022 kg/(m$^2$ s), vapor qualities from 0.03 to 0.97, reduced pressures from 0.02 to 0.80 and tube internal diameters from 3.1 to 21.4 mm. The database includes heat transfer coefficients for the following flow regimes: stratified, stratified-wavy, annular, intermittent and mist.

Regarding the experimental condensation heat transfer coefficients themselves, they are "quasi-local" data obtained in short test sections that give a mean heat transfer coefficient for a small (or sometimes even large) change in vapor quality, $\Delta x$, from inlet to outlet. The $\Delta x$ should optimally be on the order of 0.05 or less but in some tests was as large as 0.20–0.40. It would be better in the future to utilize an enthalpy profile approach to get true local heat transfer coefficients, such as described in Zürcher et al. [30] for measuring local flow boiling heat transfer coefficients. With respect to condensation heat transfer data, the most difficult test conditions to make accurate measurements are as follows:

*Near flow regime transition zones*. If a transition from one flow pattern to another takes place within the "quasi-local" test section, the mean heat transfer coefficient for the section is an unknown average of the two regimes. Also, consider that the transition from one regime to the next typically occurs over a mass velocity range of about 50 kg/(m$^2$ s), which is analogous to the transition regime in single-phase flow (where heat transfer coefficients are more difficult to measure).

*Very high and low vapor qualities*. As $x \Rightarrow 1$ and as $x \Rightarrow 0$, small errors in energy balances of $\pm 2\%$ are magnified. Typical errors in energy balances are on the order of $\pm 1\%$ to $\pm 3\%$, which represent identical errors in $x$. Referring to Fig. 4 in Part I, at low $x$ the void fraction $\varepsilon$ decreases very rapidly with small changes in $x$; e.g. a error of $\pm 0.02$ at $x = 0.03$ means that the real vapor quality could be from 0.01 or 0.05, which may result in a halving or doubling the value of $\varepsilon$, respectively. At very high $x$, $\varepsilon$ and the annular liquid film thickness $\delta$ are very sensitive to small changes in the liquid fraction $(1 - x)$; e.g. a change of just $\pm 0.01$ in $\varepsilon$ may result in a doubling or halving of the condensate film thickness. Hence, it is particularly difficult to accurately measure condensation data at vapor qualities less than 0.05 and above 0.95.

*Desuperheating and subcooling*. There is a less than obvious effect of desuperheating on the test data at high vapor qualities, caused by the condensate formed in a desuperheater before the test section, i.e. condensate formed while cooling the vapor to its saturation temperature. This condensate enters the condenser test section and hence the film begins with some initial value of $\delta_{in} > 0$ rather than starting from $\delta = 0$ at $x = 1$ and $\varepsilon = 1$. This effect tends to increase the film thickness, which in turn decreases the heat transfer coefficient measured. This "desuperheating" condensate only influences data where its preexisting fraction of the total condensate is significant, i.e. at high $x$ for say $1.0 \geqslant x \geqslant 0.9$. This may be the reason that some high vapor quality heat transfer coefficients tend to *plateau* at high vapor qualities. Secondly, some local condensation test data may include subcooling since the $\Delta x$ in the test sections during *quasi-local* experiments are often from 0.05 to 0.3 and thus data for $x < 0.05$ may be averaged over a single-phase liquid zone too.

*Stable operating conditions*. All experimental test loops have a limited range in which steady-state test conditions can be maintained. At low mass velocities, typically a threshold is reached where fluctuations in pressure and flow rate become significant. In particular, pressure fluctuations significantly influence $T_{sat}$, which is used to reduce the data, and hence the measured heat

transfer coefficient. Thus, some databases may include test data that fall below this threshold, giving unreliable test data at these unstable conditions but good data above this threshold.

*Very large and very small heat transfer coefficients*. A propagation of error analysis will always give large uncertainty in heat transfer coefficients when they are very large, i.e. at high $x$ and high mass velocity because $T_{sat} - T_w$ becomes small with respect to the measurement errors of the temperatures. Also, when heat transfer coefficients are very small, i.e. at low mass velocities, energy balances are less accurate because the change in the cooling water temperature from inlet to outlet, $\Delta T_{water}$, in the test section is small.

*Circumferential variation in heat transfer coefficients*. Condensation heat transfer coefficients are reported as mean values around the perimeter of the tube. Hence, in stratified and stratified-wavy flows where two different heat transfer mechanisms are involved, a sufficient number of thermocouples in the tube wall are required to capture a representative mean wall temperature to determine the mean heat transfer coefficient.

Thus, in summary, experimental condensation heat transfer data at very high and very low vapor qualities are the most difficult to measure accurately and reliably. It will be seen when comparing the new heat transfer model to the extensive database that these are the test conditions that tend to give the biggest prediction errors because these data have a higher experimental uncertainty.

## 4. New condensation model

### 4.1. Convective evaporation vs. convective condensation

As the starting point in developing a new flow pattern based heat transfer prediction model for condensation inside plain horizontal tubes, we shall begin with analysis of the annular flow heat transfer data. Since there is a close similarity between the convection mechanisms in annular film condensation and annular film evaporation inside tubes, the condensation data were first compared to the convective heat transfer correlation for the annular film during *evaporation* presented in Kattan et al. [3]

$$\alpha_{cb} = 0.0133 Re_L^{0.69} Pr_L^{0.4} \frac{\lambda_L}{\delta} \quad (1)$$

In this expression, the convective boiling heat transfer coefficient $\alpha_{cb}$ is that for the convective evaporation of the annular liquid film without any nucleate boiling contribution, calculated as a film flow and not as a tubular flow. For an annular flow, the annular liquid ring is assumed to be of uniform thickness around the entire internal perimeter of the tube. $Re_L$ is the liquid film Reynolds number and $Pr_L$ is the liquid Prandtl number (both defined later). Comparing this expression to the annular flow condensing data of Cavallini et al. [22,23], we observed that it systematically over predicted the data by about 15–20%. To explain this difference, as illustrated in Fig. 1, one can imagine that for an annular film with a wavy interface, evaporation will tend to thin the film at its troughs and thus enhance heat transfer while condensation will tend to fill up the troughs and reduce heat transfer. Hence, convective evaporation is not equivalent to convective condensation in annular flow as might be otherwise assumed.

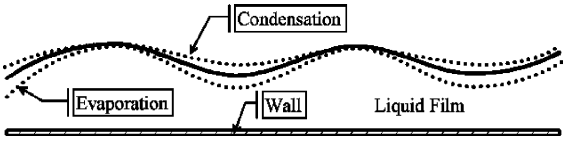


Fig. 1. Illustration of wavy interface during evaporation and condensation.

### 4.2. Simplified flow structures for condensation in horizontal tubes

The same simplified flow structures assumed for evaporation inside horizontal tubes by Kattan et al. [3] can also be applied to condensation, where the only difference is that the top to the tube in a stratified flow will be wetted by film condensation rather than remain dry during evaporation. Thus, the new condensation model proposed here assumes three simplified geometries for describing annular flow, stratified-wavy flow and fully stratified-wavy flow as shown in Fig. 2. For annular flow (bottom left), for the sake of simplicity a uniform liquid film thickness of $\delta$ is assumed and the actual larger thickness of the film at the bottom than the top due to gravity is ignored. Utilizing a void fraction equation, the cross-sectional area of the vapor phase is determined and then that of the liquid phase. From the total flow of liquid plus vapor and the local vapor quality, the mass flow rate of the liquid is calculated; then, using the liquid density and cross-sectional area occupied by the liquid, the mean velocity of the liquid is determined for the film. Hence, turbulent flow heat transfer to the film can be correlated based on the mean velocity of the liquid film, which is the standard procedure for film flows undergoing condensation, evaporation and sensible heating.

Similarly, Fig. 2 also shows the actual geometry of a fully stratified flow (upper left) and its equivalent geometry (upper right) with the same angle of stratification and cross-sectional area occupied by the liquid, but with the liquid distributed as a truncated annular ring of uniform thickness $\delta$. Fig. 3 depicts an instantaneous cross-sectional image of the liquid–vapor interface for

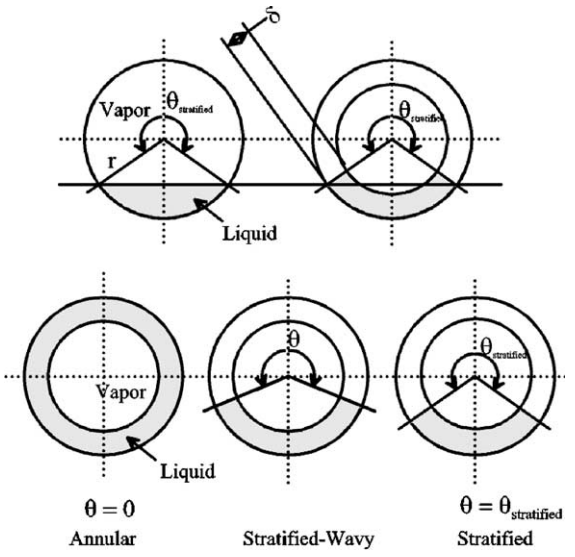


Fig. 2. Simplified flow structures for two-phase flow patterns.

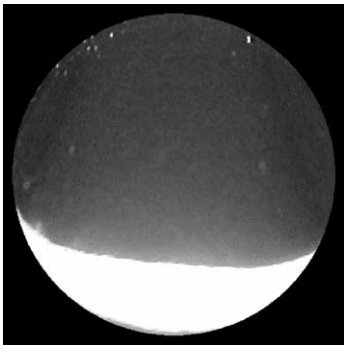

Fig. 3. Cross-sectional image of stratified-wavy flow in a horizontal tube.

an adiabatic stratified-wavy flow in a horizontal tubular sight glass of 13.6 mm internal diameter for ethanol and air obtained using a laser sheet, a video camera and image analysis by Wojtan et al. [31]. The height of the liquid on the left is a little higher than on the right because of the asynchronous height of the waves on the walls. Hence, the equivalent geometry assumed here in Fig. 2 for stratified-wavy flow is reasonably representative of the real situation.

In stratified-wavy flow, the interfacial waves are small in amplitude and do not reach the top of the tube. Hence the top perimeter of the tube is not wetted by the stratified liquid but only by the condensate that forms on this part of the exposed tube perimeter. Here, once again, for simplicity the stratified liquid is assumed to form an annular truncated ring as shown in the middle diagram at the bottom of Fig. 2. Thus, the angle $\theta$ varies between its maximum value of $\theta_{strat}$ at the threshold to fully stratified flow and its minimum value of zero at the threshold to annular flow. Notably, these three simple geometries have a smooth geometrical transition from one flow structure to another and also allow the heat transfer models to be based on the mean liquid and mean vapor velocities. In addition, the convective heat transfer coefficient can be applied to the stratified perimeter subtended by $(2\pi - \theta)$ while Nusselt film condensation can be applied to the upper wall subtended by $\theta$ with the condensate flowing downwards into the stratified liquid below. For annular flow, however, convective condensation heat transfer occurs around the entire perimeter without any Nusselt film condensation.

For simplicity's sake, the annular flow structure is also assumed to apply to the intermittent flow regime, which has a very complex flow structure, and also tentatively to the mist flow regime (assuming the impinging droplets create an equivalent unsteady liquid film). Thus, while ignoring numerous details of the actual flow structures of all these five regimes, the present geometries represent their principal features. It is then a question as to whether or not these simplified representations are sufficient to accurately model the condensation process in horizontal tubes for these five flow regimes (S, SW, I, A, MF), which will be shown to be the case. It is pertinent to note that this new model is based on *film* flow, rather than *tubular* flow, of the liquid. Most previous convective condensation models assumed tubular flow while these flows are in fact *film* flows.

Presently, no heat transfer model for the bubbly flow regime is proposed. Bubbly flows in horizontal tubes occur at very large mass velocities and hence are not commonly encountered nor are heat transfer data available for this regime.

### 4.3. Heat transfer model

Our objective here is to develop a new flow pattern/flow structure based condensation heat transfer model analogous to that which was proposed by Kattan et al. [1–3] for evaporation inside horizontal tubes. The condensation model therefore uses the same flow pattern map as for evaporation but with the new modifications introduced in Part I. Their flow pattern map for near adiabatic and evaporating flows has proved to be very accurate and reliable in comparisons to over 1000 flow pattern observations for eight different refrigerants to date. In addition, the same simplified two-phase flow structures assumed for the flow patterns in the evaporation model are also assumed for the condensation model. It is also a goal here to develop a new heat transfer model with as few empirical constants as possible. Prediction methods that include a large number of empirical parameters, some of the methods mentioned in

the literature review even have correlating equations for the empirical exponents, tend to be less reliable because they have been tightly fit statistically to the database in order to achieve small error bands. Instead, an accurate, reliable heat transfer prediction method that resorts to few empirical constants gives a good indication that the physical model "captures" the trends in the heat transfer processes.

The new condensation model assumes that two types of heat transfer mechanisms occur within the tube: convective condensation and film condensation. In the present context, convective condensation refers to the axial flow of the condensate along the channel due to the imposed pressure gradient while film condensation refers to the flow of condensate from the top of the tube towards the bottom due to gravity. Both of these mechanisms have been included in some previous models, such as that of Dobson and Chato [19]. Previous condensation models normally have assumed only two flow regimes: stratified flow and unstratified flow. Instead, it is particularly important to divide the flow into specific flow regimes: annular flow, stratified-wavy flow, fully stratified flow, intermittent flow, mist flow and bubbly flow. Only the first five are included here as little data are available for the last one while intermittent and mist flows will be treated as an annular flow for simplicity's sake.

The above two heat transfer mechanisms are applied to their respective heat transfer surface areas as shown in Fig. 4. The convective condensation heat transfer coefficient $\alpha_c$ is applied to the perimeter wetted by the axial flow of liquid film, which refers to the entire perimeter in annular, intermittent and mist flows but only part of the perimeter in stratified-wavy and fully stratified flows. The axial film flow is assumed to be turbulent. The film condensation heat transfer coefficient $\alpha_f$ is applied to the perimeter that would otherwise be dry in an adiabatic two-phase flow and hence is the upper perimeter of the tube for stratified-wavy and fully stratified flows. $\alpha_f$ is obtained by applying the Nusselt falling film theory to the inside of the horizontal tube, which assumes the falling film is laminar. The effect of axial shear on this falling film is ignored. Heat transfer coefficients for stratified types of flow are known experimentally to be a function of the wall temperature difference while those for annular flow are not. This effect will thus be included through the Nusselt falling film heat transfer equation in the present model.

The general expression for the local condensing heat transfer coefficient $\alpha_{tp}$ is

$$\alpha_{tp} = \frac{\alpha_f r\theta + (2\pi - \theta) r\alpha_c}{2\pi r} \tag{2}$$

In this expression, $r$ is the internal radius of the tube and $\theta$ is the falling film angle around the top perimeter of the tube. Hence, for annular flow with $\theta = 0$, $\alpha_{tp}$ is equal to $\alpha_c$. The stratified angle $\theta_{strat}$ is calculated from the following implicit geometric equation:

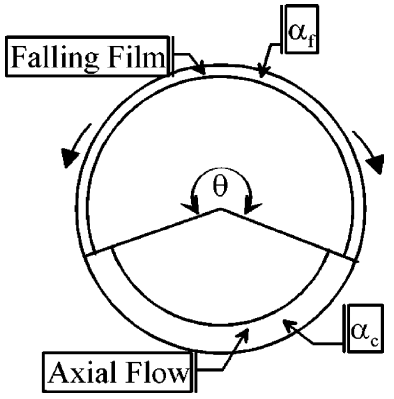


Fig. 4. Heat transfer model showing convective and falling film boundaries.

$$A_L = \frac{d^2}{8}[(2\pi - \theta_{strat}) - \sin(2\pi - \theta_{strat})] \tag{3}$$

where the cross-sectional area occupied by the liquid phase $A_L$ is

$$A_L = (1 - \varepsilon)A \tag{4}$$

and the cross-sectional area occupied by the vapor is

$$A_V = \varepsilon A = 1 - A_L \tag{5}$$

$A$ is the total cross-sectional area of the tube and $\varepsilon$ is the local vapor void fraction, which is determined using the logarithmic mean void fraction (LM$\varepsilon$) using the Rouhani and Axelsson [32] drift flux model and the homogeneous model (see Part I) in order to cover the range from low to high reduced pressures.

For annular, intermittent and mist flows, $\theta = 0$. For fully stratified flow, $\theta = \theta_{strat}$. For stratified-wavy flow, the stratified angle $\theta$ is obtained by assuming a quadratic interpolation between its maximum value of $\theta_{strat}$ at $G_{strat}$ and its minimum value of 0 at $G_{wavy}$

$$\theta = \theta_{strat}\left[\frac{(G_{wavy} - G)}{(G_{wavy} - G_{strat})}\right]^{0.5} \tag{6}$$

The values of $G_{strat}$ and $G_{wavy}$ at the vapor quality in question are determined from their respective transition equations in the flow pattern map (see Part I).

The convective condensation heat transfer coefficient $\alpha_c$ is obtained from the following turbulent film equation:

$$\alpha_c = cRe_L^n Pr_L^m \frac{\lambda_L}{\delta} f_i \tag{7}$$

where the liquid film Reynolds number $Re_L$ is based on the mean liquid velocity of the liquid in $A_L$ as

$$Re_L = \frac{4G(1-x)\delta}{(1-\varepsilon)\mu_L} \tag{8}$$

and $Pr_L$ is the liquid Prandtl number defined as

$$Pr_L = \frac{c_{pL}\mu_L}{\lambda_L} \tag{9}$$

In these expressions $c$, $n$ and $m$ are empirical constants to be determined from the heat transfer database and $\delta$ is the thickness of the liquid film. The best value of the exponent $m$ on $Pr_L$ was determined to be $m = 0.5$, which is slightly larger than that in the Dittus–Boelter single-phase flow correlation but is the same value found earlier by Labuntsov [33] for turbulent falling film condensation on a vertical plate. The best values of $c$ and $n$ for Eq. (7) were found statistically to be $c = 0.003$ and $n = 0.74$.

The liquid film thickness $\delta$ is obtained from solving the following geometrical expression:

$$A_L = \frac{(2\pi-\theta)}{8}[d^2 - (d-2\delta)^2] \tag{10}$$

where $d$ is the internal diameter of the tube. When the liquid occupies more the one-half of the cross-section of the tube in a stratified-wavy or fully stratified flow at low vapor quality, this expression will yield a value of $\delta > d/2$, which is not geometrically realistic. Hence, whenever $\delta > d/2$ then $\delta$ is set equal to $d/2$.

Analysis of the data demonstrated that an additional factor influenced convective condensation. After looking at various possibilities, the interfacial surface roughness was identified as the most influential of these effects for the following reasons. First of all, the shear of the high speed vapor is transmitted to the liquid film across the interface and hence increases the magnitude and number of the waves generated at the interface, which in turn increases the available surface area for condensation, tending to increase heat transfer. Secondly, the interfacial waves are non-sinusoidal and thus tend to reduce the mean thickness of the film, again increasing heat transfer. These two aspects are analogous to the enhancement correction factor of Kutateladze [34] for interfacial ripples on Nusselt film condensation on a vertical plate. Interfacial roughness and wave formation are also directly relatable to entrainment of liquid droplets into the vapor phase, which reduces the thickness of the liquid film and increases heat transfer. Furthermore, interfacial shear tends to create vorticies within the liquid film, which also increase heat transfer.

Applying this reasoning, the interfacial roughness can be expected to be directly proportional to the interfacial shear $\tau_i$, where $\tau_i$ in turn depends on the velocity difference between the two phases, $(u_V - u_L)$ where $u_V$ and $u_L$ are the mean velocities of the phases in their respective cross-sectional areas $A_V$ and $A_L$

$$u_L = \frac{G(1-x)}{\rho_L(1-\varepsilon)} \tag{11}$$

$$u_V = \frac{Gx}{\rho_V\varepsilon} \tag{12}$$

Since normally $u_V \gg u_L$, then $(u_V - u_L) \approx u_V$. If we normalized the vapor velocity with that of the liquid, we get the slip ratio, $u_V/u_L$, typical of void fraction models, and the interfacial shear is proportional to the term $(u_V/u_L)$. Thus, interfacial roughness $\Delta\delta_i$ can be assumed to be proportional to $(u_V/u_L)^j$ where the exponent $j$ is unknown. In addition, the one-dimensional Taylor instability wavelength $\lambda_T$ for the unsupported liquid film on the top of the tube is:

$$\lambda_T\left[\frac{(\rho_L-\rho_V)g}{\sigma}\right]^{1/2} = 2\pi\sqrt{3} \tag{13}$$

and this should also be related to the formation of interfacial waves. If the interfacial waves have characteristic wavelengths similar to the film thickness, then substituting $\delta$ for $\lambda_T$ means that the interfacial roughness $\Delta\delta_i$ will be approximately scaled as

$$\Delta\delta_i \propto \left[\frac{(\rho_L-\rho_V)g\delta^2}{\sigma}\right]^k \tag{14}$$

where the term inside the brackets is non-dimensional. Based on this reasoning, the interfacial roughness correction factor $f_i$ was introduced to act on $\alpha_c$ in Eq. (7) as follows by adjusting the exponents $j$ and $k$ based on the test data to nominal values of 1/2 and 1/4 but without introducing any empirical constants:

$$f_i = 1 + \left(\frac{u_V}{u_L}\right)^{1/2}\left(\frac{(\rho_L-\rho_V)g\delta^2}{\sigma}\right)^{1/4} \tag{15}$$

The interfacial roughness correction factor $f_i$ tends towards a value of 1.0 as the film becomes very thin (roughness must be proportional to film thickness) but $f_i$ tends to increase as the slip ratio $u_V/u_L$ increases. Finally, $f_i$ tends to decrease as $\sigma$ increases, since surface tension acts to smooth out the waves. For fully stratified flow, interfacial waves are damped out and hence the above expression becomes

$$f_i = 1 + \left(\frac{u_V}{u_L}\right)^{1/2}\left(\frac{(\rho_L-\rho_V)g\delta^2}{\sigma}\right)^{1/4}\left(\frac{G}{G_{strat}}\right) \tag{16}$$

when $G < G_{strat}$, which produces a smooth variation in $\alpha_{tp}$ across this flow pattern transition boundary just like for all the other transition boundaries and the ratio of $G/G_{strat}$ acts to damp out the effect of interfacial roughness in stratified flow.

The film condensation heat transfer coefficient $\alpha_f$ is obtained from the theory of Nusselt [35] for laminar

flow of a falling film on the internal perimeter of the tube, where $\alpha_f$ is the mean coefficient for this perimeter. Rather than integrating from the top of the tube to the stratified liquid layer at $\theta/2$ to obtain $\alpha_f$, which would be more theoretically satisfying, it was found sufficient to simply use the mean value for condensation around the perimeter from top to bottom with its analytical value of 0.728, and thus avoid a numerical integration to facilitate practical use of this method in designing condensers. Hence, $\alpha_f$ is

$$\alpha_f = 0.728\left[\frac{\rho_L(\rho_L-\rho_V)gh_{LV}\lambda_L^3}{\mu_L d(T_{sat}-T_w)}\right]^{1/4} \tag{17}$$

Since heat exchanger design codes are typically implemented assuming a heat flux in each incremental zone along the exchanger, it is more convenient to convert this expression to heat flux using Newton's law of cooling, such that the heat flux version of Nusselt's equation where the local heat flux is $q$, is given by the expression

$$\alpha_f = 0.655\left[\frac{\rho_L(\rho_L-\rho_V)gh_{LV}\lambda_L^3}{\mu_L dq}\right]^{1/3} \tag{18}$$

where the leading constant 0.655 comes from $0.728^{4/3}$. The difference in the accuracy of the predictions whether using the first or second of these expressions for $\alpha_f$ is negligible.

To completely avoid any *iterative* calculations, the recent explicit expression of Biberg [36] can be used to very accurately (error $\approx 0.00005$ rad for $2\pi \geqslant \theta_{strat} \geqslant 0$) evaluate the implicit expression above for $\theta_{strat}$, that is Eq. (3) here and Eq. (10) in Part 1:

$$\theta_{strat} = 2\pi - 2\left\{\begin{array}{l}\pi(1-\varepsilon)+\left(\frac{3\pi}{2}\right)^{1/3}[1-2(1-\varepsilon)+(1-\varepsilon)^{1/3}-\varepsilon^{1/3}] \\ -\frac{1}{200}(1-\varepsilon)\varepsilon[1-2(1-\varepsilon)][1+4((1-\varepsilon)^2+\varepsilon^2)]\end{array}\right\} \tag{19}$$

This expression gives $\theta_{strat}$ directly from the void fraction and has no effect on the location of the transition curves compared to the prior method.

The above heat transfer prediction method cannot be evaluated at $\varepsilon = 1.0$ because of division by zero. Furthermore, experimental condensation heat transfer test data will have an error in vapor quality of at least $\pm 0.01$ and hence it does not make sense that test data can be evaluated for $x > 0.99$. Thus, the above condensation prediction method is applicable when $0.99 \geqslant x$; when $x > 0.99$, then $x$ should be reset to 0.99. Also, the lower limit of applicability is for vapor qualities $x \geqslant 0.01$. Our range of test data is for $0.97 > x > 0.03$. This method provides for a smooth variation in $\alpha_{tp}$ across all the flow pattern transition boundaries without any *jump* in the value of $\alpha_{tp}$.

### 4.4. Implementation

The condensation heat transfer model is implemented as follows:

1. determine the local vapor void fraction using the LM$\varepsilon$ method (Part 1);
2. determine the local flow pattern using the flow pattern map (Part 1);
3. identify the type of flow pattern (annular, intermittent, mist, stratified-wavy or stratified in Part 1);
4. if the flow is annular or intermittent or mist, then $\theta = 0$ and $\alpha_c$ is determined with Eq. (7) and hence $\alpha_{tp} = \alpha_c$ in Eq. (2) where $\delta$ is obtained with Eq. (10) and $f_i$ is determined with Eq. (15);
5. if the flow is stratified-wavy, then $\theta_{strat}$ and $\theta$ are calculated using Eq. (3) or (19) and Eq. (6), then $\alpha_c$ and $\alpha_f$ are calculated using Eqs. (7) and (17) or (18), and finally $\alpha_{tp}$ is determined using Eq. (2) where again $\delta$ is obtained with Eq. (10) and $f_i$ is determined with Eq. (15);
6. if the flow is fully stratified, then $\theta_{strat}$ is calculated using Eq. (3) or (19) and $\theta_{strat}$ is set equal to $\theta$, then $\alpha_c$ and $\alpha_f$ are calculated using Eqs. (7) and (17) or (18), and finally $\alpha_{tp}$ is determined using Eq. (2) where $\delta$ is obtained with Eq. (10) and $f_i$ is determined with Eq. (16).

## 5. Comparison to refrigerant database

Fig. 5 shows a typical example of condensation heat transfer data plotted as a function of vapor quality at various mass velocities. The data are those of Cavallini et al. [22,23] for R-134a in an 8.0 mm tube. The heat transfer coefficients fall monotonically from large values at high vapor quality (where the annular film thickness is thinnest) to small values at low vapor qualities. The effect of mass velocity is more significant at large vapor qualities than at low vapor qualities. Hence the slope of the data curves increases with increasing mass velocity. All of these data fall within the annular or intermittent flow regimes, except at the lowest vapor qualities and mass velocities where they reach the stratified-wavy regime.

The new model was primarily developed using the heat transfer database of Cavallini et al. [22,23] and then

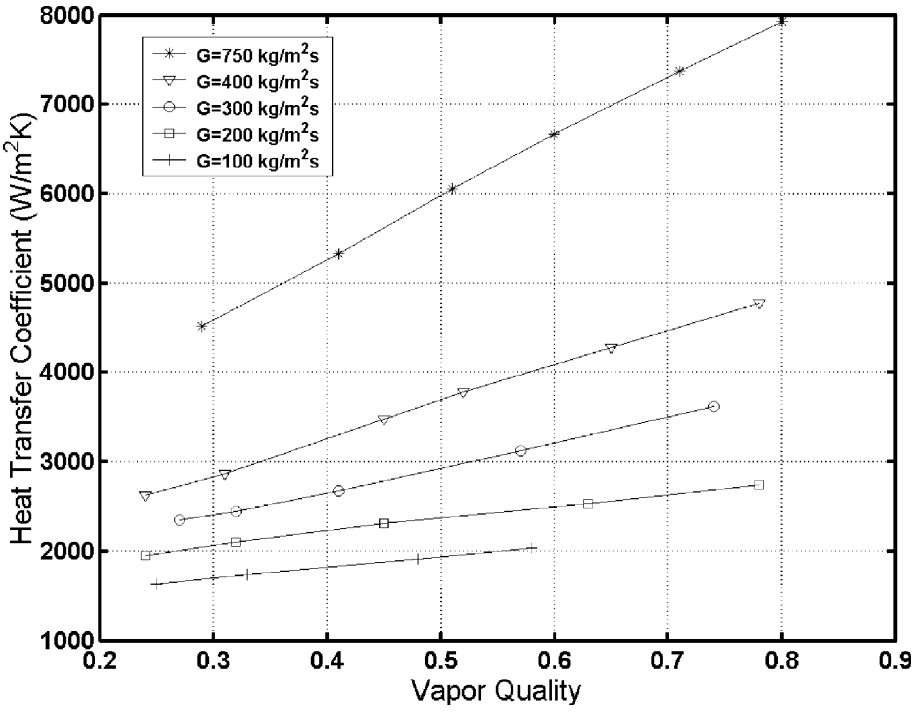


Fig. 5. Condensing data of Cavallini et al. [22,23] for R-134a.

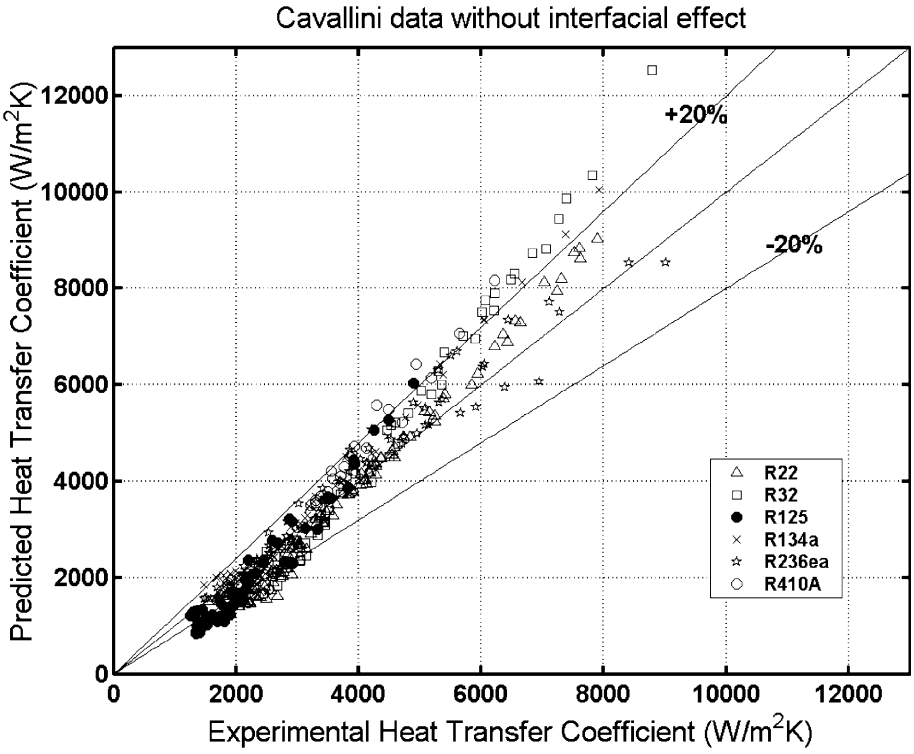


Fig. 6. Comparison of model without $f_i$ to Cavallini data.

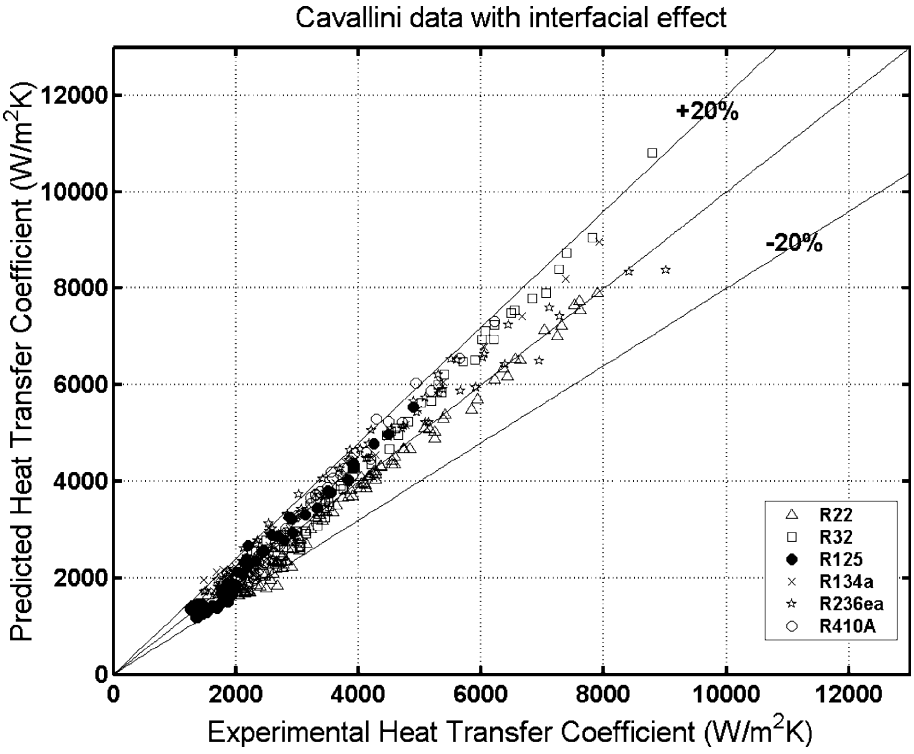


Fig. 7. Comparison of model with $f_i$ to Cavallini data.

the other independent studies were used to determine its general applicability. First of all, to demonstrate the importance of the interfacial effects in the data, Fig. 6 depicts a comparison of the new heat transfer model without use of the interfacial roughness factor (i.e. $f_i = 1.0$) and optimised to all 425 data points of Cavallini et al. [22,23] for six refrigerants, ranging from low pressure fluids (R-236ea) to high pressure fluids (R-125, R-410A and R-32). For this case, the optimum values of $c$ and $n$ are 0.0016 and 0.8585. In comparison, Fig. 7 shows the same data including $f_i$ where the optimal values are those cited in the previous section. As can be visually noted, the inclusion of the interfacial roughness factor significantly improves accuracy.

Fig. 8 depicts a comparison of the new heat transfer model to all data, except the hydrocarbon data of Kim et al. [26]. There are eleven fluids represented with a total of 1850 data points. Based on all the data points in Fig. 8 from these numerous different test facilities, about 85.0% are predicted within ±20%. A comparison to the hydrocarbon data is shown in a later section.

## 6. Parametric study on accuracy

Figs. 7 and 8 provide only a statistical view of the accuracy of the new model. However, in order to be useful as a method for the optimisation of heat exchangers, it is important that the method respect the characteristic trends in the data, i.e. the effect of individual variables on the prediction of the local heat transfer coefficient. Hence, the same data are shown in a more detailed graphical presentation below in the following graphs in which the % error $\{\%\ \text{error} = 100\% \bullet (\alpha_{pred} - \alpha_{meas})/\alpha_{meas}\}$ is plotted versus the important parameters in the model: vapor quality $x$, void fraction $\varepsilon$, liquid film thickness $\delta$, liquid Reynolds number $Re_L$, reduced pressure $p_{red}$, mass velocity $G$, tube diameter $d$, flow regime, and interfacial roughness factor $f_i$. Hence, positive values represent *over* prediction and negative values represent *under* prediction.

Fig. 9 depicts the data plotted versus vapor quality where the % error is quite evenly distributed over the range of vapor qualities. This means that the model is correctly capturing the slope of $\alpha_{tp}$ vs. $x$ as $G$ changes. The scatter is larger at very high and very low vapor qualities where measurements typically have larger errors or may include desuperheating or subcooling effects as mentioned earlier.

Fig. 10 presents the data plotted versus void fraction. As void fraction increases rapidly with vapor quality, refer for example to Fig. 4 (Part 1), most of the data is in the high void fraction range. Even so, the % errors are reasonably well distributed over the range. Data at high

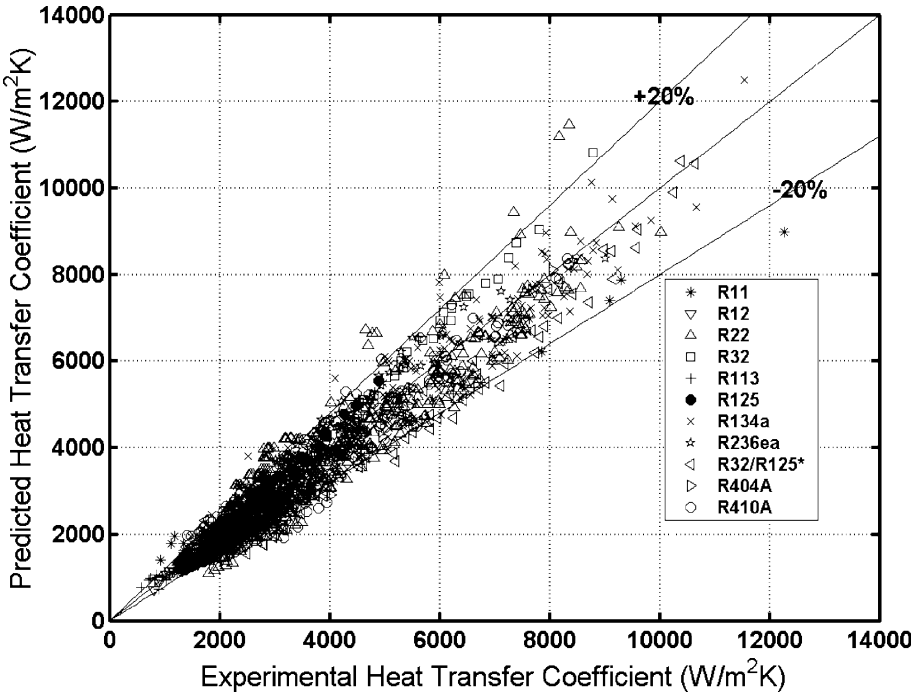


Fig. 8. Comparison of model with $f_i$ to all refrigerant data.

void fractions tend to be the most difficult to predict because a very small change of 0.005 in void fraction has a notable effect on the film thickness when the void fraction is larger than 0.95. Referring to Fig. 5, the increase in the slope of $\alpha_{tp}$ versus $x$ with increasing $G$ is the effect of $G$ on the void fraction via Eqs. (2) and (6) in Part 1. Other previous condensation models that used the Zivi [37] void fraction equation, which is independent of $G$, therefore introduced numerous empirical correction factors to account for this trend, while the present model does not require these.

Fig. 11 shows the data plotted versus the liquid film thickness. The values of $\delta$ in the database range from as low as 0.008 mm (only 8 μm!) up to as high as 8 mm (a ratio of 1000–1). The strong deviations for R-22 at low values are the high vapor quality data of Kim (see comments later on his data). The experimental data at very high vapor qualities, which result in the very small film thicknesses, will be affected by any pre-existing condensate formed during desuperheating the vapor as mentioned earlier, which will cause the model to over predict the measured heat transfer coefficients.

Fig. 12 depicts a comparison versus the liquid Reynolds number, which is a key parameter in calculating $\alpha_c$. The experimental range in $Re_L$ is from 300 to 85,000. The deviations in the data are well centered around the 0% error line when plotted versus this parameter.

Fig. 13 depicts the important comparison of the new model to test data versus reduced pressure. The lowest pressure represented in the database is 78 kPa while the highest is 3184 kPa. The new model works just as well at low reduced pressures as at high ones, that is from 0.02 to 0.8, while previous prediction methods are not reliable over such a wide range.

Fig. 14 shows the % errors plotted versus mass velocity. The range in mass velocities here is very large, 24–1022 kg/(m$^2$ s), and the new model predicts the entire range with good accuracy. The band of errors is somewhat larger at low mass velocities since these flows are in the stratified-wavy and fully stratified regimes, or in annular or intermittent flow near the transition, where the prediction of the heat transfer coefficient is sensitive to the calculation of the dry angle and the $G_{wavy}$ flow pattern transition, respectively.

Fig. 15 illustrates the prediction errors as a function of tube internal diameter. The range of internal diameters represented is very broad, i.e. from 3.1 to 21.4 mm, which covers nearly all the sizes of the heat transfer tubes used in industrial practice. The predictions for most of the tube sizes are pretty well centered around 0% error. At the smallest diameter, the capillary effects in the flow pattern map on flow pattern transitions and heat transfer may start to play a role, since this size may be in the *mesoscale* between *macrochannels* and *microchannels*.

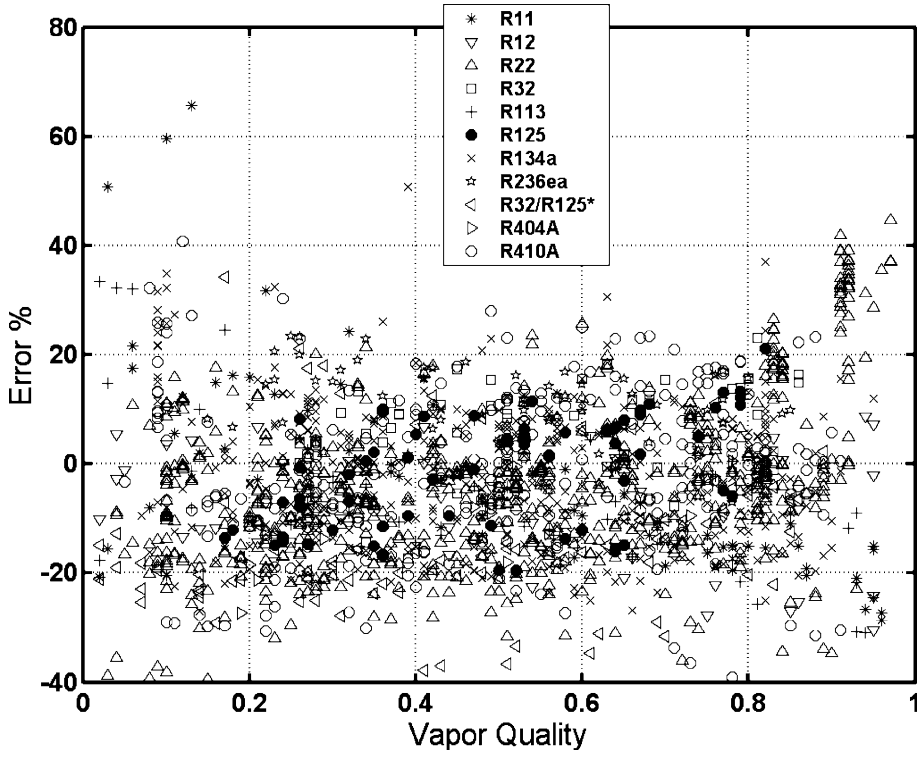


Fig. 9. Comparison of model plotted versus vapor quality.

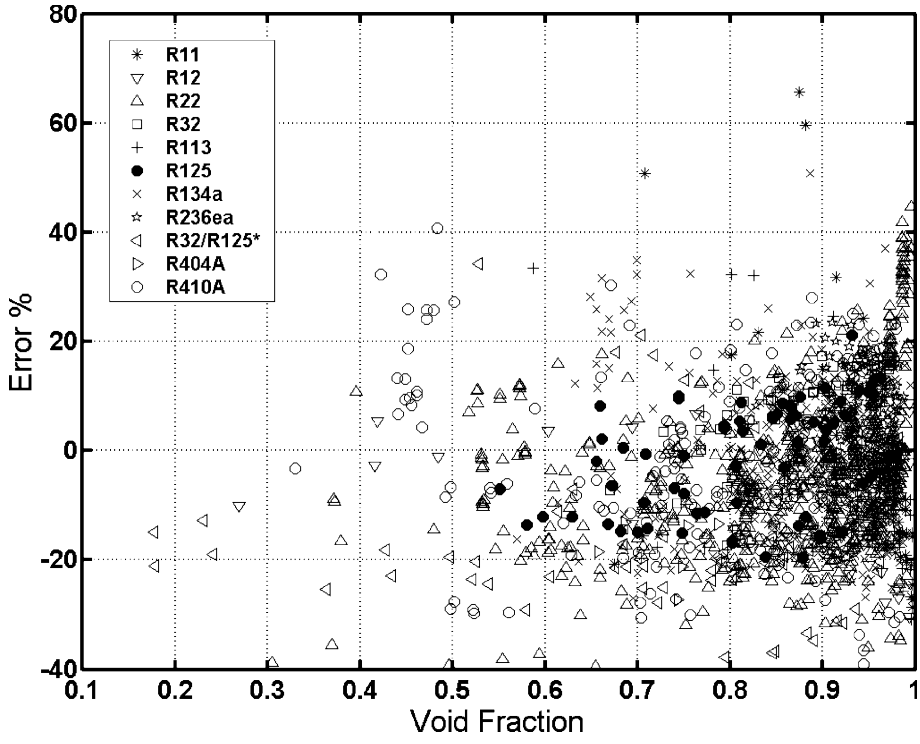


Fig. 10. Comparison of model plotted versus void fraction.

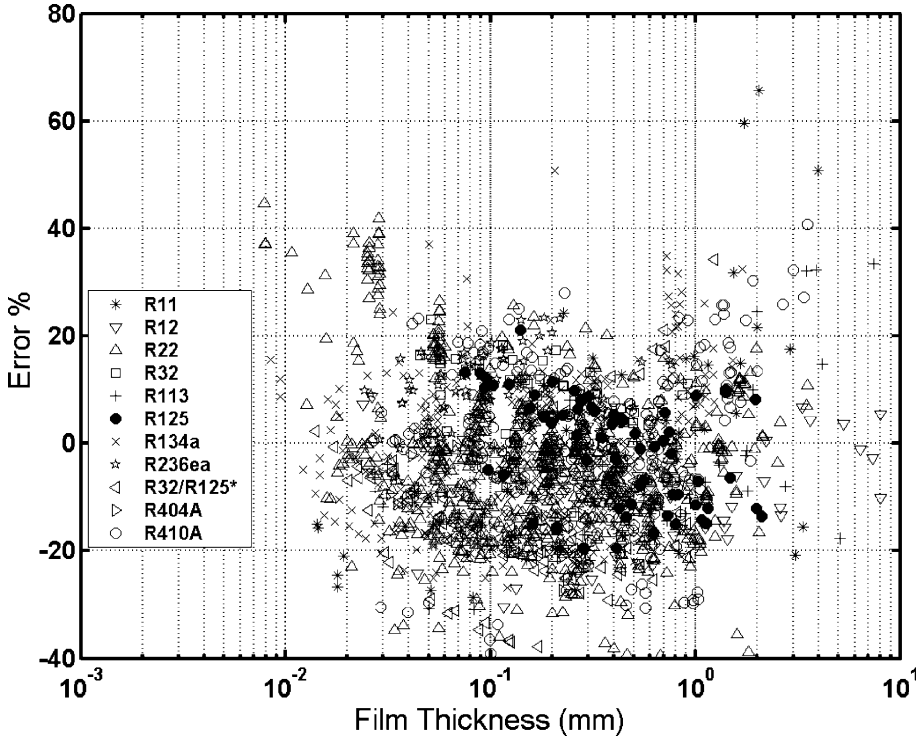


Fig. 11. Comparison of model plotted versus film thickness.

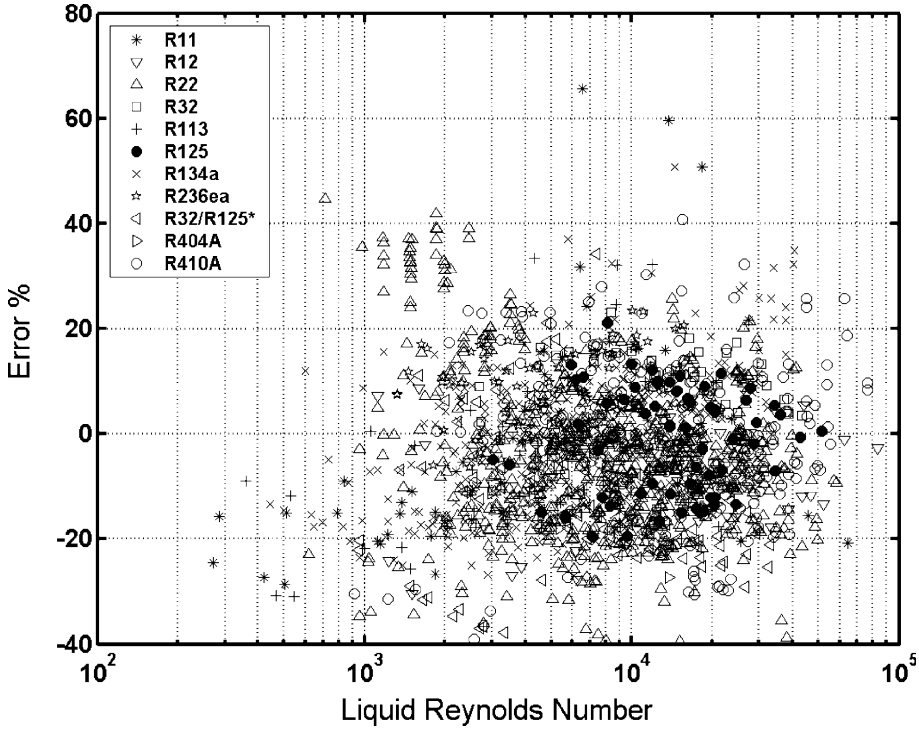


Fig. 12. Comparison of model plotted versus liquid Reynolds number.

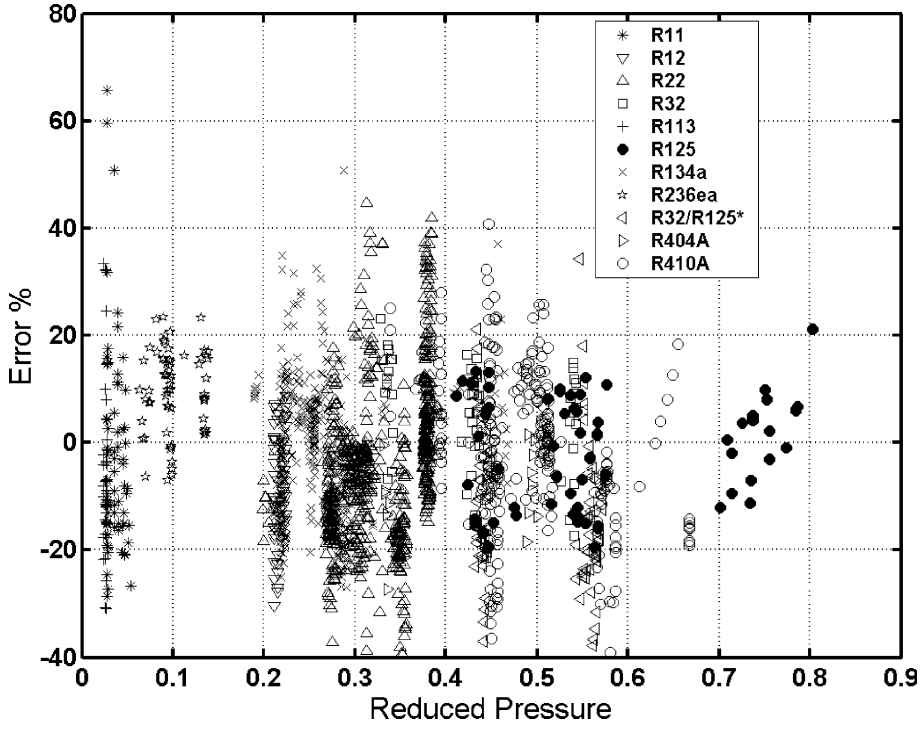


Fig. 13. Comparison of model plotted versus vapor reduced pressure.

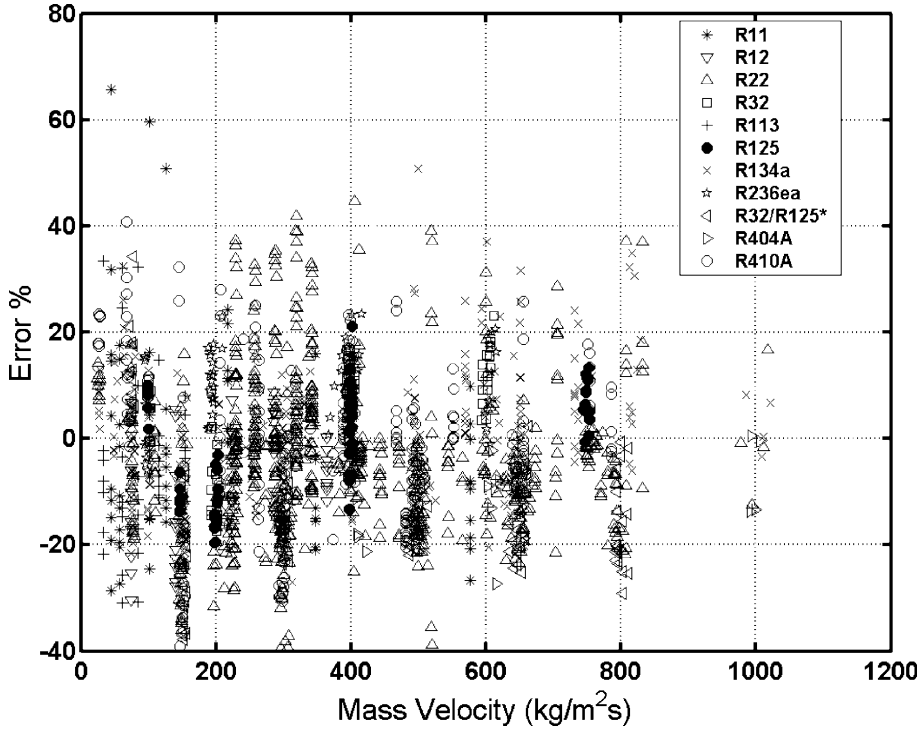


Fig. 14. Comparison of model plotted versus mass velocity.

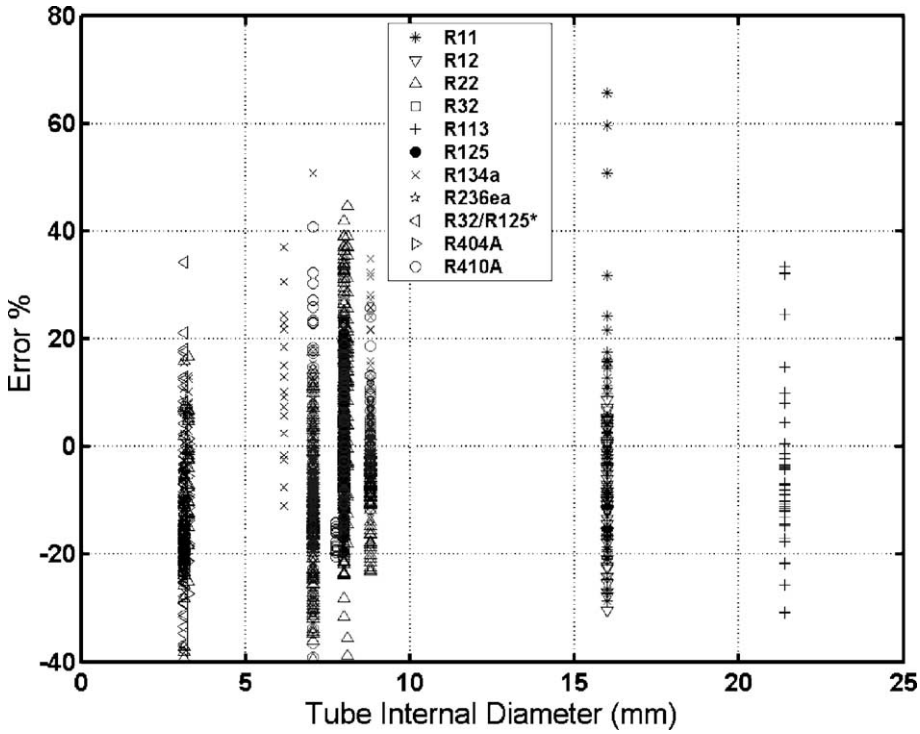


Fig. 15. Comparison of model plotted versus tube diameter.

Fig. 16 shows the breakdown of how the new model works by individual flow regime (S = fully stratified flow, SW = stratified-wavy flow, I = intermittent flow, A = annular flow and MF = mist flow). First of all, it is seen that the method works about equally well for all the flow regimes, as indicated by how the data scatter around the 0% error line. The stratified regime is the only one a little off center and those data are some of the most difficult to predict and measure (e.g. it is difficult to maintain steady-state conditions and get good energy balances at these very low mass velocities and also the variation in the falling film heat transfer coefficient around the perimeter of the tube may not be captured correctly unless 8–10 thermocouples are used). Also, it is seen that applying the annular flow heat transfer structure to intermittent flow works just as well as for annular flow itself.

Regarding mist flow, which was *not* originally one of the flow regimes planned to be modelled here, applying the annular flow heat transfer structure ($\theta = 0$) gives a surprisingly good prediction for these few data (nine points) that are above the mist flow transition boundary ($G_{mist}$). Apparently, what this means physically is that reformation of the condensate film is very rapid on the wall where liquid has been stripped off into the mist. Not many data are often measured at this high of mass velocity, so we have also compared the new model to some very old data that are available in the mist flow regime for R-12 (21 points) at 757 and 1532 kg/(m$^2$ s) and R-22 (2 points) at 1002 kg/(m$^2$ s) from Travis et al. [12], classifying their data using the mist flow transition equation of the flow pattern map in Part 1. These mist flow heat transfer coefficients are predicted reasonably well, under predicting their values by about 15–20%. However, while it is interesting to see that the annular flow heat transfer model seems to work surprisingly well, not enough data are available to develop a separate mist flow heat transfer model at present.

Fig. 17 shows the range of interfacial roughness factor $f_i$ in the database and the % error plotted versus this parameter. The test data have also been plotted versus the wall temperature difference, $(T_{sat} - T_w)$, but these are not shown here. The plot shows that the % error tends to increase as the temperature difference becomes smaller, similar to the propagation of error in the experiments.

## 7. Comparison to hydrocarbons

Addressing now condensation of hydrocarbons, such data are only available from a single source, Kim et al. [26]. In addition to their tests on R-22, they tested propane, *n*-butane, iso-butane and propylene in an

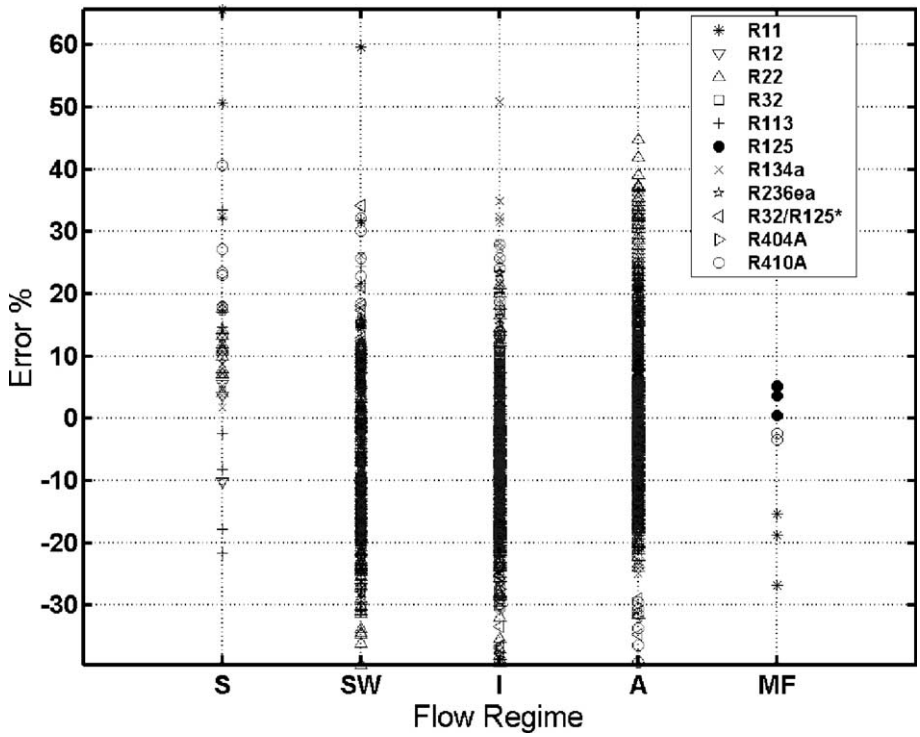


Fig. 16. Comparison of model by flow pattern.

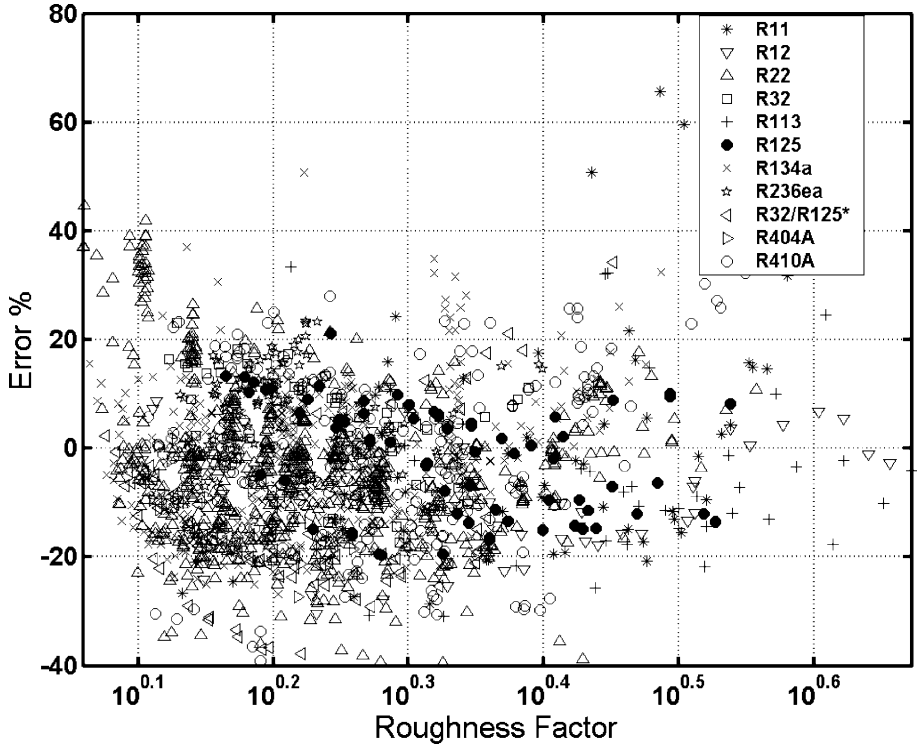


Fig. 17. Comparison of model plotted versus interfacial roughness factor.

8.0 mm tube. Their experimental technique is similar to others and they quote good experimental accuracy. Fig. 18 shows their data plotted versus vapor quality, where the predictions are much poorer for some of the hydrocarbons than for R-22, and Fig. 19 plots their data sets for their lowest mass velocity for each of their five fluids. It is seen that their test data exhibit an unusual levelling off or even a minimum at high vapor qualities, which is not seen in any of the other data sets in the database for refrigerants, e.g. compare these trends to Fig. 5 at high vapor qualities. Hence, there seems to be an experimental problem with the Kim data in the high vapor quality range. Also, Fig. 20 shows all their data plotted versus mass velocity. It is seen that their data also exhibit a strong deviation only at low mass velocities, for those below about 100–120 kg/(m$^2$ s). Hence, again there appears to be an unidentified experimental problem (for example, energy balances or flow instabilities as mentioned earlier) with data in this lower flow range, compared to the earlier comparison in Fig. 14, which showed good agreement with numerous independent data sets at low $G$. Thus, overall, the new heat transfer model seems to work well for hydrocarbons in the range that the Kim data follow the expected trends of the other data sets, for which the large majority are predicted within ±20%. Compared to all the refrigerant data plus all Kim's hydrocarbon data (2771 points), the new model predicts 75% of the data to within ±20%. On the other hand, if we simply eliminate all the Kim data for mass velocities less than 100 kg/(m$^2$ s), where his data deviate from all others (refer to Fig. 20 with respect to predictions), then the model retains its high accuracy also for hydrocarbons.

## 8. Statistical comparison

Table 2 provides a statistical summary of the comparison of the new heat transfer model to the experimental database. The data are classified by flow regime to show their distribution. The errors reported in Cavallini et al. [20] for the comparison of their method to parts of the current database are also shown in brackets for comparison purposes. They did not compare their method to the hydrocarbon data nor to the Fujii data. Statistically, the two methods give nearly the same accuracy while the new model here is also shown to work well for the data of Fujii and Liebenberg for refrigerants and for the hydrocarbon data of Kim. The values in the table for the hydrocarbons are not really representative since all the data were included, even those with the unusual trends pointed out earlier.

In summary, the new heat transfer model involves only six basic equations (Eqs. (2), (6), (7), (15) or (16), (17) or (18) and the void fraction from Part 1) plus auxiliary equations to define dimensionless numbers and

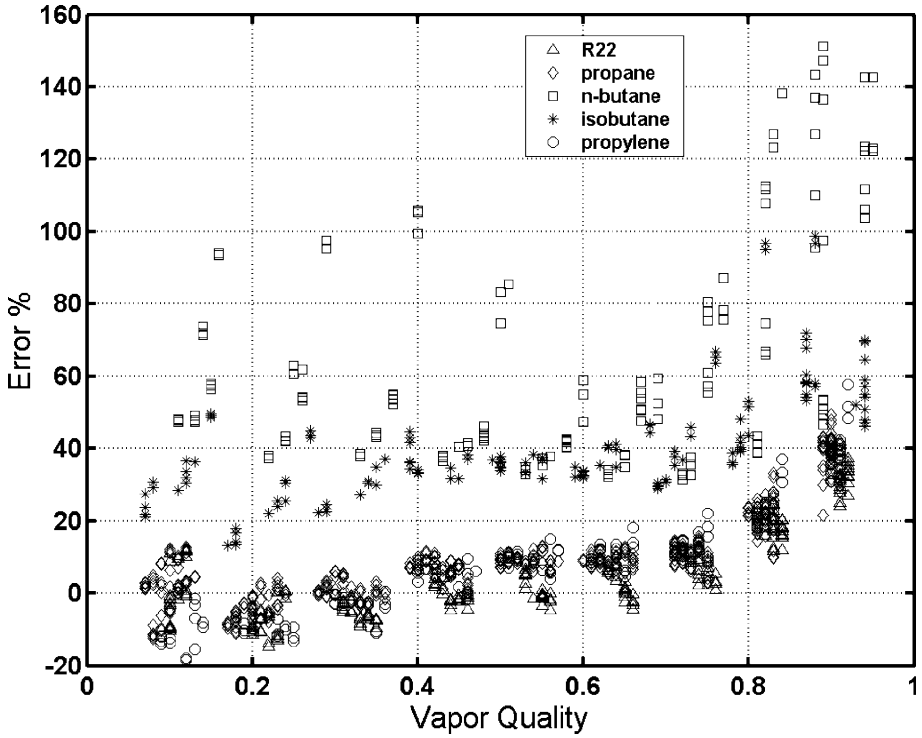


Fig. 18. Comparison to hydrocarbon data versus vapor quality.

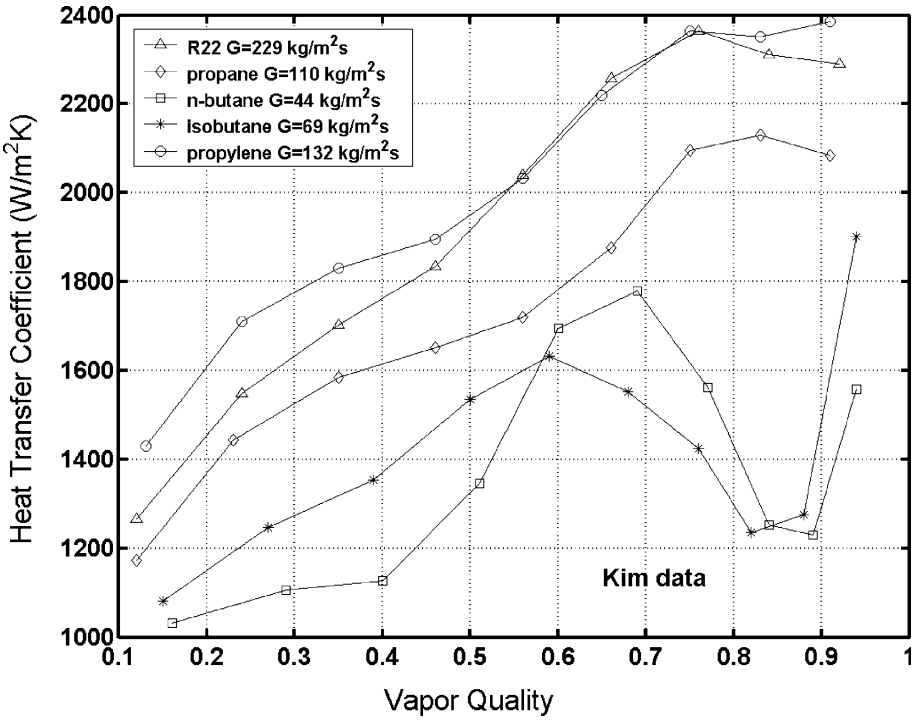


Fig. 19. Hydrocarbon heat transfer data at low mass velocities.

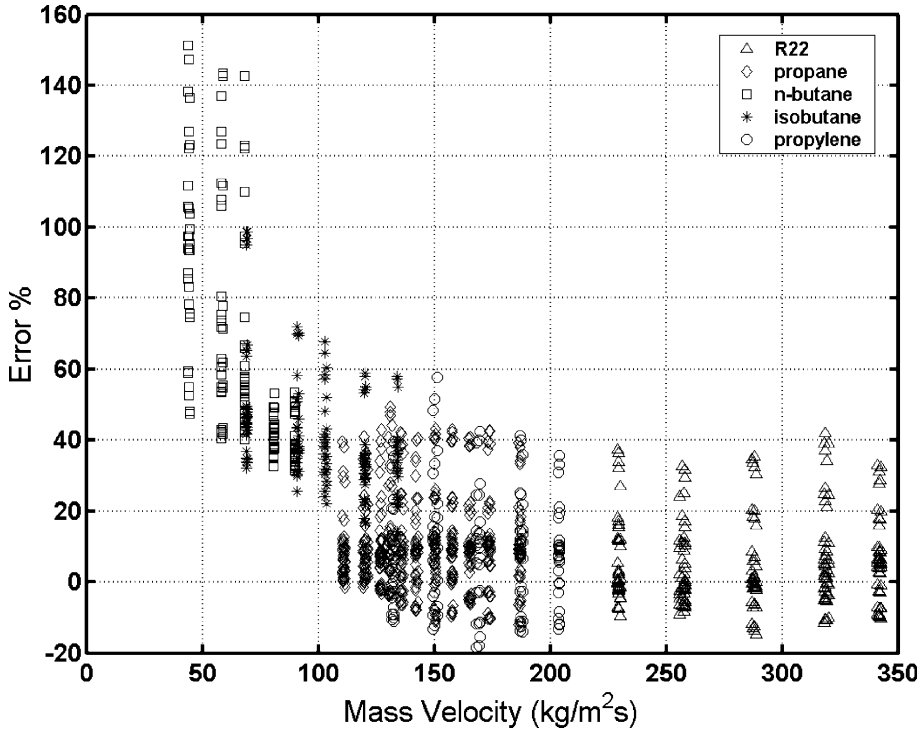


Fig. 20. Hydrocarbon data comparison plotted versus mass velocity.

Table 2
Statistical information by flow regime and source

| Author | Fluid | Present model (Cavallini et al. model) | | | | | | | | | | | | | | | | | | | |
|---|---|---|---|---|---|---|---|---|---|---|---|---|---|---|---|---|---|---|---|---|---|
| | | Number of points | | | | | Mean error | | | | | Arithmetic error | | | | | Standard deviation | | | | |
| | | S | SW | I | A | MF | S | SW | I | A | MF | S | SW | I | A | MF | S | SW | I | A | MF |
| Cavallini | R22 | 1 | 21 | 33 | 51 | | 7 | 13 | 7 | 7 | | 8 | −13 | −6 | −6 | | 0 | 9 | 7 | 7 | |
| | | | | 106 *(106)* | | | | | 8 *(5)* | | | | | −8 *(−5)* | | | | | 8 *(3)* | | |
| | R134a | 1 | 19 | 23 | 31 | | 32 | 11 | 7 | 8 | | 32 | 1 | 1 | 8 | | 0 | 13 | 8 | 5 | |
| | | | | 74 *(74)* | | | | | 9 *(4)* | | | | | 4 *(4)* | | | | | 10 *(5)* | | |
| | R410A | | 11 | 20 | 22 | | | 9 | 9 | 13 | | | 2 | 1 | 12 | | | 10 | 10 | 7 | |
| | | | | 53 *(53)* | | | | | 11 *(6)* | | | | | 6 *(5)* | | | | | 10 *(5)* | | |
| | R125 | | 25 | 25 | 19 | 4 | | 12 | 5 | 11 | 4 | | −9 | 1 | 4 | 4 | | 10 | 6 | 11 | 2 |
| | | | | 73 *(73)* | | | | | 9 *(5)* | | | | | −2 *(0)* | | | | | 10 *(6)* | | |
| | R236ea | | 14 | 7 | 45 | | | 6 | 18 | 11 | | | 4 | 18 | 10 | | | 7 | 5 | 7 | |
| | | | | 66 *(66)* | | | | | 11 *(5)* | | | | | 10 *(2)* | | | | | 8 *(7)* | | |
| | R32 | | 10 | 19 | 24 | | | 8 | 9 | 12 | | | −1 | 3 | 10 | | | 9 | 10 | 8 | |
| | | | | 53 *(53)* | | | | | 10 *(5)* | | | | | 5 *(4)* | | | | | 10 *(4)* | | |
| Dobson & Chato | R22 | 11 | 62 | 81 | 92 | | 11 | 17 | 19 | 12 | | 11 | −15 | −19 | −11 | | 4 | 13 | 6 | 6 | |
| | | | | 246 *(246)* | | | | | 15 *(12)* | | | | | −14 *(−8)* | | | | | 10 *(12)* | | |
| | R134a | 10 | 76 | 44 | 66 | | 8 | 10 | 13 | 12 | | 8 | −7 | −11 | −11 | | 4 | 10 | 12 | 8 | |
| | | | | 196 *(196)* | | | | | 11 *(11)* | | | | | −8 *(−8)* | | | | | 11 *(9)* | | |
| | R410A | 9 | 21 | 40 | 36 | | 23 | 14 | 14 | 10 | | 23 | 4 | −14 | −10 | | 8 | 17 | 9 | 12 | |
| | | | | 106 *(106)* | | | | | 14 *(12)* | | | | | −6 *(−9)* | | | | | 16 *(12)* | | |
| | R32/R125(60/40%) | | 17 | 46 | 33 | | | 14 | 21 | 13 | | | 6 | −21 | −13 | | | 15 | 6 | 9 | |
| | | | | 96 *(96)* | | | | | 17 *(12)* | | | | | −13 *(−6)* | | | | | 13 *(13)* | | |
| Tang | R22 | | | 42 | 48 | | | | 12 | 5 | | | | −12 | −5 | | | | 7 | 3 | |
| | | | | 90 *(73)* | | | | | 8 *(12)* | | | | | −8 *(−12)* | | | | | 6 *(7)* | | |
| | R134a | | | 34 | 42 | | | | 15 | 4 | | | | 12 | 3 | | | | 13 | 4 | |
| | | | | 76 *(66)* | | | | | 9 *(8)* | | | | | 7 *(0)* | | | | | 10 *(11)* | | |
| | R410A | | | 39 | 11 | 2 | | | 7 | 2 | 3 | | | 4 | 1 | −3 | | | 9 | 2 | 1 |
| | | | | 52 *(34)* | | | | | 5 *(14)* | | | | | 3 *(1)* | | | | | 8 *(16)* | | |
| Zhang | R22 | | | 10 | 13 | | | | 10 | 7 | | | | −7 | −2 | | | | 10 | 8 | |
| | | | | 23 *(23)* | | | | | 8 *(9)* | | | | | −4 *(5)* | | | | | 10 *(11)* | | |
| | R134a | | | 18 | 20 | | | | 8 | 11 | | | | 1 | 11 | | | | 11 | 10 | |
| | | | | 38 *(38)* | | | | | 10 *(11)* | | | | | 7 *(10)* | | | | | 11 *(8)* | | |
| | R404A | | | 9 | 7 | | | | 14 | 6 | | | | −14 | −6 | | | | 7 | 7 | |
| | | | | 16 *(16)* | | | | | 11 *(6)* | | | | | −11 *(−3)* | | | | | 8 *(7)* | | |
| Chitti &Anand | R410A | | | 20 | 21 | | | | 8 | 10 | | | | −4 | 9 | | | | 11 | 9 | |
| | | | | 41 *(12)* | | | | | 9 *(14)* | | | | | 3 *(7)* | | | | | 12 *(26)* | | |
| Wijaya | R410A | | | 10 | 4 | | | | 17 | 17 | | | | −17 | −17 | | | | 2 | 2 | |
| | | | | 14 *(7)* | | | | | 17 *(27)* | | | | | −17 *(−27)* | | | | | 2 *(1)* | | |
| Fujii | R11 | 3 | 40 | 3 | 20 | 3 | 45 | 14 | 9 | 11 | 20 | 45 | −4 | 4 | −5 | −20 | 25 | 17 | 12 | 12 | 6 |
| | | | | 69 | | | | | 14 | | | | | −2 | | | | | 19 | | |

| | | | | | | | | | | | | | | | | | | | | |
|---|---|---|---|---|---|---|---|---|---|---|---|---|---|---|---|---|---|---|---|---|
| | R12 | 3 | 28 | 4 | 15 | 6 | 15 | 3 | 5 | 0 | −14 | 0 | −1 | 9 | 10 | 5 | 6 | | | |
| | | | | 50 | | | | 10 | | | | −8 | | | | 11 | | | | |
| | R113 | 8 | 26 | | 5 | 20 | 13 | | 6 | 8 | −9 | | −4 | 23 | 12 | | 7 | | | |
| | | | | 39 | | | | 13 | | | | −5 | | | | 16 | | | | |
| Kim | R22 | | 35 | 65 | 125 | | 6 | 6 | 13 | | 1 | −5 | 12 | | 7 | 5 | 13 | | | |
| | | | | 225 | *(225)* | | | 10 | *(15)* | | | 5 | *(12)* | | | 13 | *(12)* | | | |
| | Propane | | 95 | 152 | 248 | | 4 | 6 | 19 | | 1 | 3 | 19 | | 5 | 7 | 12 | | | |
| | | | | 495 | | | | 12 | | | | 10 | | | | 13 | | | | |
| | *n*-Butane | | 144 | | | | 65 | | | | 65 | | | | 32 | | | | | |
| | | | | 144 | | | | 65 | | | | 65 | | | | 32 | | | | |
| | iso-Butane | | 76 | 9 | 62 | | 39 | 31 | 45 | | 39 | 31 | 45 | | 20 | 6 | 12 | | | |
| | | | | 147 | | | | 41 | | | | 41 | | | | 17 | | | | |
| | Propene | | 9 | 61 | 65 | | 6 | 8 | 22 | | −6 | −2 | 22 | | 4 | 9 | 13 | | | |
| | | | | 135 | | | | 14 | | | | 9 | | | | 16 | | | | |
| | R22 | | | 24 | 24 | | 13 | 23 | | | 0 | 23 | | | 16 | 11 | | | | |
| Liebenberg | | | | 48 | | | | 18 | | | | 12 | | | | 18 | | | | |

the flow structure. In these expressions, there is only *one* empirical constant, $c$ in Eq. (7), and there is only *one* empirical exponent, $n$ in Eq. (7), plus those of three exponents whose values were assumed, i.e. for $j$ ($=1/2$), $k$ ($=1/4$) and 1/2 for the interpolation in Eq. (6). Also, the exponent $m$ on the Prandt number $Pr_L$ was adjusted from its tubular flow value of 0.4 to its film flow value of 0.5, similar to Labuntsov [33]. Thus, the use of the flow pattern map to categorize the flow regimes, the simplified flow structures to describe the flow regimes, and a reliable void fraction equation to predict liquid film thickness results in a simple heat transfer model that is accurate and valid over a wide range of conditions without resorting to statistical tweaking of the model's equations.

## 9. Simulations for R-410A

To illustrate the predicted trends in $\alpha_{tp}$ as a function of vapor quality and mass velocity, the heat transfer model and flow pattern map have been simulated for R-410A condensing at 40 °C in an 8 mm diameter tube assuming a heat flux of 40 kW/m$^2$. The flow pattern map is shown in Part 1 while the heat transfer coefficients are shown in Fig. 21. At the lowest flow rate, 30 kg/(m$^2$ s), the flow is in the stratified regime from inlet to outlet and the heat transfer coefficient falls off slowly with decreasing vapor quality. At 200 kg/(m$^2$ s), the flow enters in annular flow and then passes through intermittent and stratified-wavy flow. At 500 kg/(m$^2$ s), the flow enters in the annular flow regime and converts to intermittent flow at about $x = 0.55$ and leaves in this same regime. The sharp decline in $\alpha_{tp}$ at high vapor qualities results from the rapid growth of the annular film thickness. At 800 kg/(m$^2$ s), the flow enters in the mist flow regime, goes then into the annular flow regime and then leaves in the intermittent regime. As can be seen, the new heat transfer model predicts the variation in the local heat transfer coefficients across flow pattern transition boundaries without any discontinuity in the value of $\alpha_{tp}$. This, for example was a problem in the Dobson and Chato [19] method and also for one of the transitions in the more recent Cavallini et al. [20] method going into their slug flow regime. Also of note, the heat transfer coefficient would exhibit a small peak in the SW zone at 200 kg/(m$^2$ s) if the same simulations were repeated for Fig. 21 at a low heat flux, such as 10 kW/m$^2$, since then $\alpha_f$ around the top of the tube would be larger than $\alpha_c$ around the bottom of the tube.

## 10. Condensation of mixtures

The above method is extendable to the prediction of local condensation heat transfer coefficients of zeotropic

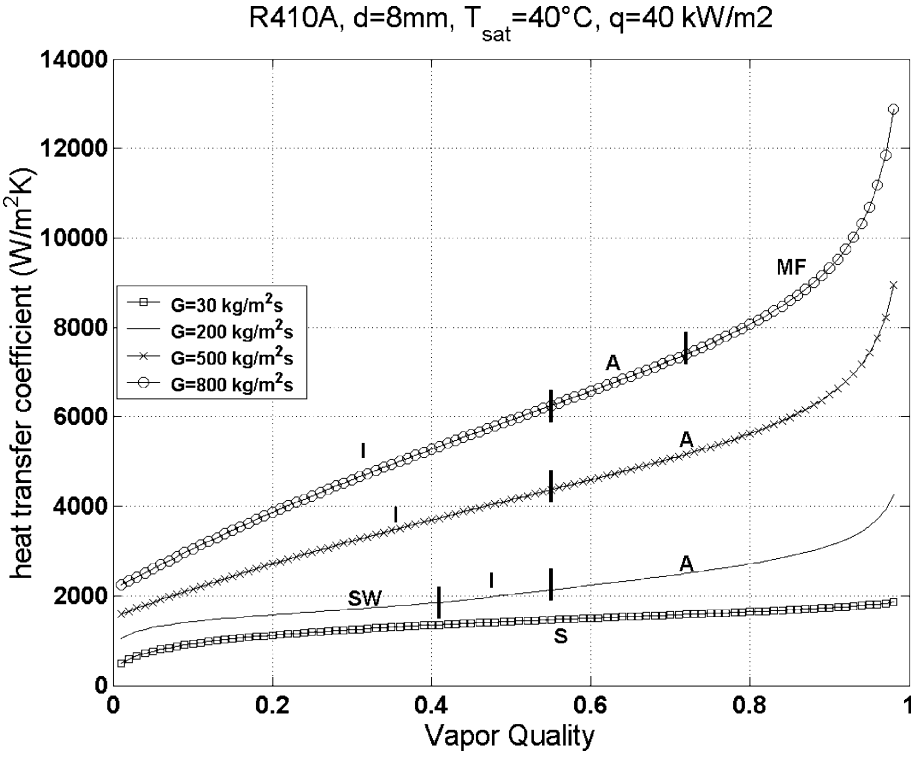


Fig. 21. Simulation of model for condensation of R-410A.

mixtures or for condensation in the presence of non-condensable gases by use of the Bell and Ghaly [38] method. This method essentially consists of assuming two thermal resistances in series: the first resistance is for convective heat transfer in the vapor-phase from the bulk vapor temperature to the temperature at the vapor–liquid interface and the second resistance is across the condensate film itself, given by $1/\alpha_{tp}$. Comparison to such test data is beyond the present scope and will be treated in a future study.

## 11. Conclusions

A new general flow pattern based heat transfer model for condensation inside horizontal, plain tubes has been proposed here based on the same simplified flow structures of the flow regimes used in the flow boiling model of Kattan et al. [3]. The condensation heat transfer model includes the effect of interfacial roughness of the liquid–vapor on heat transfer. The model resorts to very few empirical constants and exponents compared to other previous methods. The model accurately predicts local condensation heat transfer coefficients for the following flow regimes: annular, intermittent, stratified-wavy, fully stratified and mist flow. It accurately predicts a very broad experimental database for fifteen fluids obtained in nine different laboratories. The new model has so far been tested for the following range of conditions: mass velocities from 24 to 1022 kg/(m$^2$ s), vapor qualities from 0.03 to 0.97, reduced pressures from 0.02 to 0.80 and tube internal diameters from 3.1 to 21.4 mm. Overall, the method predicts 85% of the refrigerant heat transfer coefficients in the database (1850 points) to within ±20% and predicts 75% of the refrigerant plus hydrocarbon heat transfer coefficients in the database (2771 points) to within ±20%.

## Acknowledgements

A. Cavallini participated in this project as an ER-COFTAC Scientific Visitor to the Laboratory of Heat and Mass Transfer in Lausanne and we are grateful to him for providing the majority of the database used in this project.

## References

[1] N. Kattan, J.R. Thome, D. Favrat, Flow boiling in horizontal tubes: part 1—development of a diabatic two-phase flow pattern map, J. Heat Transfer 120 (1998) 140–147.

[2] N. Kattan, J.R. Thome, D. Favrat, Flow boiling in horizontal tubes: part 2—new heat transfer data for five refrigerants, J. Heat Transfer 120 (1998) 148–155.
[3] N. Kattan, J.R. Thome, D. Favrat, Flow boiling in horizontal tubes: part 3—development of a new heat transfer model based on flow pattern, J. Heat Transfer 120 (1998) 156–165.
[4] H. Jaster, P.J. Kosky, Condensation heat transfer in a mixed flow regime, Int. J. Heat Mass Transfer 19 (1976) 95–99.
[5] F.W. Dittus, M.L.K. Boelter, Heat transfer in automobile radiators of the tubular type, University of California Publications on Engineering, Berkeley, CA 2(13), 1930, p. 443.
[6] W.W. Akers, H.A. Deans, O.K. Crosser, Condensing heat transfer within horizontal tubes, Chem. Eng. Progr. Symp. Series 55 (1959) 171–176.
[7] W.W. Akers, H.F. Rosson, Condensation inside a horizontal tube, Chem. Eng. Progr. Symp. Series 56 (1960) 145–149.
[8] ASHRAE Handbook—Fundamentals, ASHRAE, Atlanta, GA, 2001, 4–10.
[9] A. Cavallini, R. Zecchin, High velocity condensation of organic refrigerants inside tubes, in: Proceedings 13th International Congress of Refrigeration, vol. 2, 1971, pp. 193–200.
[10] A. Cavallini, R. Zecchin, A dimensionless correlation for heat transfer in forced convection condensation, in: Proceedings Sixth International Heat Transfer Conference, vol. 3, 1974, pp. 309–313.
[11] P.J. Kosky, F.W. Staub, Local condensing heat transfer coefficients in the annular flow regime, AIChE J. 17 (1971) 1037–1043.
[12] D.F. Traviss, M.W. Rohsenow, A.B. Baron, Forced convection inside tubes: a heat transfer equation for condenser design, ASHRAE Trans. 79 (1972) 157–165.
[13] D. Butterworth, Film condensation of pure vapor, in: Heat Transfer Design Handbook, Begell House, New York, 1993.
[14] Condensation within horizontal tubesVDI Heat Atlas, D.5, VDI-Verlag GmbH, Düsseldorf, 1993, pp. 13–16.
[15] Kondensation an waagerechten Rohren, VDI-Wärmeatlas 8. Auflage 1997, D4, VDI-Verlag GmbH, Düsseldorf, 1997, 7–9.
[16] M.M. Shah, A general correlation for heat transfer during film condensation inside pipes, Int. J. Heat Mass Transfer 22 (1979) 547–556.
[17] L. Tang, Empirical study of new refrigerant flow condensation inside horizontal smooth and micro-fin tubes. Ph.D. Thesis, University of Maryland at College Park, 1997.
[18] H. Haraguchi, S. Koyama, T. Fujii, Condensation of refrigerants HCFC22, HFC134a and HCFC123 in a horizontal smooth tube (2nd report, proposal of empirical expressions for local heat transfer coefficient), Trans. JSME 60 (574) (1994) 245–252.
[19] M.K. Dobson, J.C. Chato, Condensation in smooth horizontal tubes, J. Heat Transfer 120 (1998) 193–213.
[20] A. Cavallini, G. Censi, D. Del Col, L. Doretti, G.A. Longo, L. Rossetto, In-tube condensation of halogenated refrigerants, ASHRAE Trans. 108 (1) (2002), Paper 4507.
[21] L. Friedel, Improved friction pressure drop correlations for horizontal and vertical two-phase pipe flow, European Two-phase Flow Group Meeting, Ispra, Italy, 1979, Paper E2.
[22] A. Cavallini, D. Del Col, G.A. Longo, L. Rossetto, Condensation heat transfer with refrigerants, in: Proceedings of the Two-Phase Flow Modelling and Experimentation Conference, ETS, Pisa, vol. 1, 1999, pp. 71–88.
[23] A. Cavallini, D. Del Col, G.A. Longo, L. Rossetto, Experimental investigation on condensation heat transfer and pressure drop of new HFC refrigerants (R134a, R125, R32, R410A, R236ea) in a horizontal tube, Int. J. Refrig. 24 (2001) 73–87.
[24] M. Zhang, A new equivalent Reynolds number model for vapour shear-controlled condensation inside smooth and micro-fin tubes, Ph.D. Thesis, Pennsylvania State University, University Park, PA, 1998.
[25] M.S. Chitti, N.K. Anand, Condensation heat transfer inside smooth horizontal tubes for R-22 and R-32/125 mixture, Int. J. HVAC&R Res. 2 (1996) 79–101.
[26] M.S. Kim, Y.S., Chang, S.T. Ro, Performance and heat transfer of Hydrocarbon refrigerants and their mixtures in a heat pump system, in: Proceedings of IIR-IIF Meeting of Commissions B1, B2, E1 and E2 Applications for Natural Refrigerants, Aarhus, Denmark, 1996, pp. 477–486.
[27] H. Wijaya, M.W. Spatz, Two-phase flow heat transfer and pressure drop characteristics of R-22 and R-32/125, ASHRAE Trans. 101 (1) (1995) 1020–1027.
[28] T. Fujii, personal communication to A. Cavallini, 1993.
[29] L. Liebenberg, Condensation performance in smooth and enhanced tubes, Ph.D. thesis, Department of Mechanical Engineering, Rand Afrikaans University, 2002.
[30] O. Zürcher, J.R. Thome, D. Favrat, Evaporation of ammonia in a smooth horizontal tube: heat transfer measurements and predictions, J. Heat Transfer 121 (1999) 89–101.
[31] L. Wojtan, T. Ursenbacher, J.R. Thome, Technique for measurement of void fraction in horizontal tubes, in: Compact Heat Exchangers and Enhancement Technology for the Process Industries—2001, Begell House, New York, 2001, pp. 353–360.
[32] Z. Rouhani, E. Axelsson, Calculation of void volume fraction in the subcooled and quality boiling regions, Int. J. Heat Mass Transfer 13 (1970) 383–393.
[33] D.A. Labuntsov, Heat transfer in film condensation of steam on a vertical surface and horizontal tubes, Teploenergetika 4 (7) (1957) 72–80.
[34] S.S. Kutateladze, Fundamentals of Heat Transfer, Academic Press, New York, 1963.
[35] W. Nusselt, Die oberflachenkondensation des wasserdampfes, Z. Ver. Dt. Ing. 60 (1916) 541–546, 569–575.
[36] D. Biberg, An explicit approximation for the wetted angle in two-phase stratified pipe flow, Canadian J. Chemical Engineering 77 (1999) 1221–1224.
[37] S.M. Zivi, Estimation of steady state void fraction by means of minimum entropy production, J. Heat Transfer 86 (1964) 247–252.
[38] K.J. Bell, M.A. Ghaly, An approximate generalized design method for multicomponent/partial condenser, AIChE Symp. Ser. 69 (1973) 72–79.